Electrochemical Promotion of Catalysis for the hydrogenation of CO_2 to valuable fuels and chemicals

Synopsis of ELECTROFUELS ARISTEIA PROJECT

Abstract

The kinetics and the electrochemical promotion of the hydrogenation of CO_2 to CH_4 and CO is compared for Ru porous catalyst films deposited on Na^+, K^+, H^+ and O^{2-} conducting solid electrolyte supports. It is found that in all four cases increasing catalyst potential and work function enhances the methanation rate and selectivity. Also in all four cases the rate is positive order in H_2 and exhibits a maximum with respect to CO_2. At the same time the reverse water gas shift reaction (RWGS) which occurs in parallel exhibits a maximum with increasing p_{H_2} and is positive order in CO_2. Also in all cases the selectivity to CH_4 increases with increasing p_{H_2} and decreases with increasing p_{CO_2}. These results provide a lucid demonstration of the rules of chemical and electrochemical promotion which imply that $(\partial r/\partial\Phi)(\partial r/\partial p_D) > 0$ and $(\partial r/\partial\Phi)(\partial r/\partial p_A) < 0$, where r denotes a catalytic rate, Φ is the catalyst work function and p_D, p_A denote the electron donor and electron acceptor reactant partial pressures respectively.

1. Introduction

The hydrogenation of CO_2 to hydrocarbons is a reaction of great potential technological and environmental importance since it can lead to the production of renewable fuels but could also serve as a means for decreasing the overall CO_2 emissions. Several metals have been investigated as catalysts, including Pt, Rh, Pd, Ru, Fe, Co and Ni on a variety of supports including SiO_2, Al_2O_3, ZrO_2 and Nb_2O_3. Work in this area has been reviewed recently [1-4]. The hydrogenation of CO_2 on Ru, which is known to give only CH_4 and CO as products, has received considerable attention in recent years [5-8].

At temperatures up to 450 ^{o}C the CH_4 selectivity reaches 100% while the main byproducts are CO and traces of C2 hydrocarbons [6, 7]. Müller et al. studied the CO_2 methanation on a commercial Ru-based catalyst (RuO_2 dispersed on sintered Al_2O_3 pellets) and found an activation energy of 79 kJ/mol while Weatherbee and Bartholomew studied the hydrogenation of CO_2 on Ru/SiO_2 (0.5% Ru) and found an activation energy of 72 kJ/mol at ambient pressure and 103 kJ/mol at 11 atm [9, 10]. Ru based catalysts with high metal dispersion were studied by Kowalczyk et al. giving the following sequence of TOFs concerning the methanation reaction: Ru/Al_2O_3>$Ru/MgAl_2O_4$>Ru/MgO>Ru/C [11].

Although the dissociative adsorption of CO_2 to CO and O has been suggested in the past to be the initial step for the CO_2 hydrogenation on Ru, it is now believed that both CH_4 and CO formation proceed via intermediate formation of a formate species at the metal-support interface. The formation and accumulation of this species has been demonstrated via IR spectroscopy [5, 7, 12-14].

A parallel approach to classical chemical promotion is the electrochemical promotion of catalysis (EPOC) or non-Faradaic electrochemical modification of catalytic activity (NEMCA effect) that can be used to promote the catalytic properties of metal catalyst films simultaneously acting as electrodes, which are deposited on solid electrolyte supports, either pure ionic conductors, such as yttria-stabilized-zirconia (YSZ, an O^{2-} conductor) Na-β″-Al_2O_3, (a Na^+ conductor), or K-β″-Al_2O_3, (a K^+ conductor) or mixed ionic-electronic conductors, such as TiO_2 or CeO_2 [15-21]. Electrochemical promotion allows for continuous in situ control of the coverage of promoting species ($Na^{\delta+}$, $K^{\delta+}$, $O^{\delta-}$) on the catalyst surface.

EPOC has been investigated extensively during the last 30 years for more than 100 catalytic reaction systems using a variety of metal catalysts (or conductive metal oxides), solid electrolytes and catalytic reactions. Work in this area has been reviewed several times in recent years [18, 19, 22-27].

Numerous surface science and electrochemical techniques have shown that EPOC is due to an electrochemically controlled migration (spillover or more commonly reverse-spillover or backspillover) of promoting ionic species (e.g. O^{2-} in the case of YSZ, Na^+ or K^+ in the case of β"-Al_2O_3), from the ionic or mixed ionic-electronic conductor-support to the gas exposed catalyst surface, through the catalyst-gas-electrolyte three phase boundaries (tpb) [18, 22-31]. Thus, both catalytic activity

and selectivity are affected in a pronounced, reversible, and, to some extent, predictable manner [18, 24]. The close connection between EPOC, classical chemical promotion and metal-support interaction (MSI) with ionically conducting supports has been established by a variety of techniques [18, 22, 26, 32-35].

Two parameters are commonly used to quantify the magnitude of EPOC [18]:

1. the rate enhancement ratio, ρ, defined by Equation (1):

$$\rho = r / r_o \tag{1}$$

in which r is the electropromoted catalytic rate and r_o is the unpromoted rate (i.e. the open-circuit catalytic rate), and

2. the apparent Faradaic efficiency, Λ, defined by Equation (2):

$$\Lambda = \Delta r_{catalytic} / (I / F) \tag{2}$$

where $\Delta r_{catalytic}$ is the current- or potential-induced observed change in catalytic rate (in g-eq/s), and I is the applied current. In the present case, accounting for the stoichiometry of the methanation and of the reverse water-gas shift (RWGS) reactions, i.e.

$$CO_2 + 4H_2 \rightarrow CH_4 + 2H_2O \tag{3}$$

$$CO_2 + H_2 \rightarrow CO + H_2O \tag{4}$$

this implies

$$\Lambda_{CH_4} = 8\Delta r_{CH_4} / (I / F) \tag{5}$$

$$\Lambda_{CO} = 2\Delta r_{CO} / (I / F) \tag{6}$$

where r_{CH_4} is in mol CH_4/s and r_{CO} is in mol CO/s.

The catalyst potential, U_{WR}, is the potential of the catalyst (working electrode, denoted W) with respect to a reference electrode, denoted R [18]. The applied current, I, flows between the catalyst and a counter electrode.

A reaction is termed electrophobic (or nucleophilic) when the rate increases with increasing catalyst potential ($\partial r/\partial U_{WR}>0$), electrophilic when the rate decreases with increasing catalyst potential ($\partial r/\partial U_{WR}<0$), volcano-type when the reaction rate exhibits a maximum with varying potential, and inverted volcano when the rate goes through a minimum with varying potential [18]. The catalyst potential U_{WR} is an increasing function of the work function, Φ, of the catalyst surface and over wide temperature ranges the two are related via [16, 18, 26]:

$$\Delta\Phi = e\Delta U_{WR} \quad (7)$$

It has been found that simple rules exist, valid both for classical promotion and for electrochemical promotion [36-38], which allow for the prediction of the promotional behavior on the basis of the open-circuit reaction kinetics with respect to the electron donor (D) and electron acceptor (A) reactant species.

The electrochemical promotion of CO_2 hydrogenation has been studied on Ru catalyst films interfaced with YSZ [39, 40], Na-β″-Al_2O_3 [40], K- β″-Al_2O_3 [41] and $BaZrO_{0.85}Y_{0.15}O_{3-\alpha}$ (BZY) [42], a H^+ conductor. The adsorption of Na [43, 44] and K [45, 46] on Ru(001) has been investigated thoroughly in the past [43-46].

Lambert and coworkers have shown that adsorbed Na and K introduced via electrical potential application across solid electrolyte supports is identical to that introduced via the gas phase [19]. They have also shown that during EPOC studies in presence of H_2O and CO_2, most of the alkali atoms are in the form of adsorbed hydroxides and carbonates. Since, however, the large dipole moment of K and Na is of the order of 10 Debye and thus is typically a factor of 5 larger than that of the counter ions [47], the promotional activity of K and Na remains practically the same as in the absence of their counter ions [18, 19].

In the present work we discuss the similarities of the kinetic and EPOC results of these four studies and we compare them quantitatively with the rules of electrochemical promotion which allow for the prediction of the sign of the rate vs catalyst potential or work function behavior on the basis of the unpromoted kinetics [36-38].

In addition the hydrogenation of CO_2 using TiO_2 supported Ru and Co catalysts had been investigated. The aim of this work is the comparison of the catalysts to each other, as well as the comparison to a bimetallic Ru/Co/TiO_2 catalyst. Considering that Ru catalysts are highly selective towards methane and exhibit high conversion and Co lead to a higher number of hydrocarbon products, but with a lower conversion, the aim of the bimetallic catalyst is the achievement of both higher conversion and higher number of hydrocarbon products simultaneously.

2. Experimental

2.1. EPOC studies

The solid electrolytes were discs of 8 mol% Y_2O_3-stabilized ZrO_2 (YSZ) with 18 mm diameter and 2 mm thickness provided by Ceraflex, discs of β″-Al_2O_3 with 20 mm diameter and 3 mm thickness provided by Ionotec and discs of BZY ($BaZr_{0.85}Y_{0.15}O_3$ + 1 w% NiO) with a diameter of 18 mm and a thickness of 2 mm provided by NorECs AS. Gold organometallic paste (Metalor, A1118) was used for the deposition of the Au counter and reference electrodes on one side of the discs, followed by calcination in air at 650^{o}C for 1 hr. Blank experiments showed that gold was catalytically inactive both for the methanation and the RWGS reaction. The Ru catalyst films were deposited on the other side of the discs, via impregnation of a 150mM $RuCl_3$ solution in isopropanol at 50^{o}C, followed by calcination in air at 500^{o}C for 1 hr. The loading of the catalysts was ~1 mg for Ru/Na-β″-Al_2O_3 and Ru/BZY, ~2 mg for Ru/K-β″-Al_2O_3 and ~3 mg Ru/YSZ. Prior to any hydrogenation activity measurements, a reduction pretreatment in 5% H_2/He was performed at 300^{o}C for 1 hr.

The reaction was carried out in a continuous flow single pellet reactor analyzed in detail in previous papers [40, 41]. The catalyst pellet was placed inside a quartz tube closed at one end of volume 70 cm^3. The three electrodes (all exposed to the reaction mixture) were connected via Au wires with a potentiostat-galvanostat. The feed gas composition and total gas flow rate, F_t, were controlled by electronic flow meters (Brooks). Reactants were certified standards of 3% CO_2 in He and 30% H_2 in He. Pure He (99.999%) was fed to further adjust the total flow rate and the inlet gas composition at desired levels. All experiments were carried out at between 100 and 400 cm^3/min total volumetric gas flow rate and under atmospheric pressure. The H_2/CO_2 ratio was varied between 1 and 15. Reactants and products were analyzed by on-line gas chromatography (using Porapaq QS and Moleculer Sieve 5A columns) in conjunction with an IR CO_2-CO-CH_4 analyzer (Fuji Electric). Constant currents or potentials were applied using an AMEL 2053 galvanostat-potentiostat.

Catalyst characterization information has been provided in previous publications [39-41]. The catalytic surface area of the Ru/YSZ and the Ru/BZY catalyst films were estimated using the galvanostatic transient technique, by

measuring the time constant, τ, required for the rate increase, Δr, in potentiostatic electropromotion rate transients to reach 63% of its steady-state value [18, 39, 40, 42]. In this way one can estimate the reactive oxygen or hydrogen uptake, N_G, of the anodically polarized metal film. Assuming a 1:1 surface metal active site: O or 2H ratio, the active catalyst surface area, N_G, expressed in mol metal, can be calculated during current imposition via [18, 26]:

$$N_G = \frac{I\tau}{2F} \quad (8)$$

Using eq. (8) and constant current, i.e. galvanostatic, transients, N_G was calculated to be ~$5x10^{-7}$ mol for the Ru/YSZ catalyst and ~$1.1x10^{-7}$ mol for the Ru/BZY [39, 40, 42].

The surface area of the Ru/Na-β"-Al_2O_3 and Ru/K-β"-Al_2O_3 catalysts was estimated using galvanostatic transients in conjunction with the Helmholz equation and Faraday's law as described in previous studies [18, 48].

Substituting the slope dU_{WR}/dt, taken from the galvanostatic transient experiments, and using the applied current, I, the dipole moment values of Na on Ru(001) ($P_{o,Na} = 2\times10^{-29}$ C·m or 6 Debye [47]) or the dipole moment value of K on Ru(001) ($P_{o,K} = 4.6\times10^{-29}$ C·m or 13.8 Debye [47]) one can compute the N_G values for the Ru/Na-β"-Al_2O_3 and Ru/K-β"-Al_2O_3 catalysts which, assuming an 1:1 adsorption stoichiometry, equal 4×10^{-7} mol and 1.4×10^{-6} mol respectively. The above N_G values have been used to compute turnover frequencies, (TOFs).

2.2. Catalytic studies of supported catalysts (powders)

The experiments took place in a fixed-bed reactor over the temperature range of 140 - 460 ^oC and under total pressure up to 7 bar. Before every experiment, each sample had been reduced under H_2 10% mixture (rest: He) flow at a temperature of 400 ^oC. For every experiment the feed flow was fixed at 100 ml/min and included the reactants in concentrations of 7% for H_2 and 1% for CO_2 (rest: He). The main products of the Ru catalyst were CH_4 and CO, while higher alcanes appeared with the use of Co catalysts. The bimetallic catalyst led to an even higher number of hydrocarbons than Co (up to hexane), preserving the high conversion of the Ru catalyst at the same time.

All catalysts were prepared via wet impregnation. Initially, a precursor aqueous solution was prepared (~70 ml) (Ruthenium (III) nitrosylnitrate, Ru 31.1% min, Alfa Aesar and Cobalt (II) nitrate, Alfa) in an appropriate concertation that would lead to the final desirable w/w loading of the catalyst, and after that the support powder was added (5g TiO_2 P25, Degussa). Then, the mixture was transferred to the spherical bottle of a rotary evaporator, where it remained at an average temperature of ~60-70 ^oC and total pressure of 50 mbar and under continuous rotation, until total removal of the water. After the collection of the residual powder from the walls of the bottle, it remained for a short period of time (10 - 15 min approx.) in a dryer with dehydrating means at a temperature of 100 ^oC. Finally, the catalyst was calcinated at 500 oC for 1 h in atmospheric air.

The reactor was a piece of gas carrying ¼" stainless steel tube. Inside the reactor, at about the half of its total length, a glass cotton piece was fixed to support the catalyst bed. Also, for the control of the temperature of reactor, a thermoelement was placed in the reactor, with its ending right above the bed. This was connected to a thermocontroller, which controlled the operation of the furnace. The reactants feed system consisted of high pressure gas cylinders and mass flow meters for the control of the reactants flow.

The products analysis system consisted of a Shimatzu GC-2010 Plus gas chromatograph equipped with a ValcoPlot Alumina capillary column and an FID detector for the measurement of the hydrocarbon products and a Fuji Electric Gas Analyzer (IR) for the measurement of CO_2 and CO.

All experiments conducted at steady state and at a temperature range of 140 – 460 ^oC (at 40 ^oC intervals) and pressure up to 7 bar (achieved with the use of a leak valve at the reactor outlet). Every sample consisted of 200 mg of catalyst and it was reduced under H_2 10% mixture (rest: He) flow at a temperature of 400 ^oC prior to experiment. The feed flow was fixed at 100 ml/min and included the reactants in concentrations of 7% for H_2 and 1% for CO_2 (rest: He).

3. RESULTS AND DISCUSSION

3.1. EPOC studies

3.1.1 Overview of kinetic and promotional behavior on Ru/YSZ

Figures 1a and 1b refer to the Ru/YSZ catalyst and depict the dependence of the rate of methanation, r_{CH_4}, and of CO formation, r_{CO}, on the partial pressures of H_2, p_{H_2}, (Fig. 1a) and CO_2, p_{CO_2}, (Fig. 1b). One observes that the rate of methanation is positive order in H_2, i.e. $(\partial r_{CH_4} / \partial p_{H_2}) > 0$ and negative order in CO_2, i.e. $(\partial r_{CH_4} / \partial p_{CO_2}) < 0$.

According to the promotional rules [36-38], this implies that the methanation reaction is electrophobic (nucleophilic), i.e. one expects $(\partial r_{CH_4} / \partial U_{WR}) > 0$, as is indeed experimentally observed (Fig. 1c).

Similarly one observes in Figures 1a and 1b that the rate of CO formation via the RWGS reaction is negative order in H_2, i.e. $\partial r_{CO} / \partial p_{H_2} < 0$ and positive order in CO_2, i.e. $\partial r_{CO} / \partial p_{CO_2} > 0$. According to the promotional rules, this implies that the RWGS reaction is electrophilic, i.e. $(\partial r_{CO} / \partial U_{WR}) < 0$, as is indeed experimentally observed (Figure 1c).

3.1.2 Methanation kinetics

Figure 2 shows the dependence of the rate of methanation on the hydrogen partial pressure, p_{H_2}, for all four catalysts, i.e. Ru/YSZ, Ru/BZY(H^+), Na-β″-Al_2O_3 and K -β″-Al_2O_3. One observes that in all four cases and for low p_{H_2} values the kinetics are positive order in H_2, i.e. $\partial r_{CH_4} / \partial p_{H_2} > 0$, both for the unpromoted state and under polarization. For the case of YSZ and BZY supports the unpromoted state corresponds to zero applied current or potential, denoted in Figure 2 as o.c. (open circuit). In the case of the Na-β″-Al_2O_3 and K-β″-Al_2O_3 solid electrolyte supports, the unpromoted state corresponds to a cleaned surface, which is obtained after positive potential application (U_{WR}=0.8 V) for 30 min.

One may also observe in Figure 2 that in the case of the O^{2-} and H^+ conducting supports, where the rate remains positive order in H_2 for high p_{H_2} values as well, the

rate of methanation is an increasing function of catalyst potential $(\partial r / \partial U) > 0$, i.e. the reaction is electrophobic, whereas in the case of the Na^+ and K^+-conducting supports where the rate levels off with increasing p_{H_2}, the rate passes through a maximum with potential, i.e. the rate exhibits volcano type behavior.

Figure 3 shows the dependence of the rate of methanation, r_{CH_4}, on the CO_2 partial pressure p_{CO_2}. One observes that the rate exhibits a maximum, which implies strong adsorption of CO_2, and is zero to negative order in CO_2 for $p_{CO_2} > 1$ kPa, i.e. $(\partial r_{CH_4} / \partial p_{CO_2} < 0)$. The rate maximum is well known to correspond to roughly equal coverages of the adsorbed reactants [18]. One can also observe in Fig. 3 that for the case of the O^{2-} and H^+ conducting supports the rate increases monotonously with potential $(\partial r_{CH_4} / \partial U_{WR}) > 0$, i.e. electrophobic behavior is observed, whereas in the case of the Na^+ and K^+ supports the rate goes through a maximum i.e. it exhibits volcano-type behavior.

3.1.3 Kinetics of RWGS reaction

The kinetics of the reverse water-gas shift (RWGS) reaction, (equation (4)) are depicted in figures 4 and 5. The rate vs p_{H_2} dependence is shown in Figure 4. One observes that the rate is zero or negative order in H_2 for p_{H_2} values above 2 kPa.

On the other hand, the rate of the RWGS reaction is always positive order in CO_2 for all four supports as shown in Figure 5.

One may also observe in Figures 4 and 5 that the rate of CO formation decreases monotonously with increasing potential (electrophilic behaviour, i.e. $(\partial r_{CO} / \partial U_{WR}) < 0$) for all four supports.

3.1.4 Selectivity dependence on gas composition

As a consequence of the results of sections 3.1.2 and 3.2,3, the selectivity to CH_4, denoted S_{CH_4}, increases significantly with increasing p_{H_2} (Fig. 6) while the selectivity to CO, S_{CO}, exhibits exactly the opposite behaviour.

For the cases of YSZ and BZY supports this increase in selectivity is dramatic, i.e. from 10% to 90% in the case of YSZ and from ~0% to 88% for the case BZY at U_{WR}=0.5 V, (Fig. 6).

It is also evident from Figure 6 that increasing potential causes in general an increase in S_{CH_4} and a decrease in S_{CO}, a point which is further elaborated below.

3.1.5 Rate dependence on temperature, catalyst potential and work function

The activation energy for CO formation, E_{CO}, was found to be 71 kJ/mol for Ru/YSZ (in the temperature range 260-320^{o}C), while both E_{CO} and the corresponding value for CH_4 formation, E_{CH_4}, was found to be 92 kJ/mol for Ru/BZY in the range 330 to 450^{o}C and 75 to 79 kJ/mol for Ru/K-β″-Al_2O_3 in the range 300 to 380^{o}C. These values are in reasonable agreement with the literature values of 72 kJ/mol for Ru/SiO_2 [10] and 79 kJ/mol for Ru/Al_2O_3 [9] for finely dispersed supported Ru catalysts.

The key characteristics of the rate dependence on catalyst potential are already evident from Figures 1 to 5 and are shown in more detail in Figure 7. The rate of CO formation decreases monotonically with increasing potential for all four catalyst supports, i.e. electrophilic behavior is obtained $(\partial r / \partial U_{WR}) < 0$.

On the other hand, the rate of methanation increases monotonically with potential (nucleophilic behavior, $\partial r / \partial U_{WR} > 0$) only for the YSZ and BZY supports (Fig. 7). In the case of the Na-β″-Al_2O_3 and K-β″-Al_2O_3 supports, the rate of methanation, r_{CH_4}, exhibits a maximum with increasing potential, i.e. it exhibits volcano-type behaviour as shown in Figure 7. This is also evident from Figure 8 which depicts the potential dependence of the turnover frequencies, TOF_{CH4} and TOF_{CO} on catalyst potential U_{WR}. The second potential axis, $U_{WR(Na)}$ in these Figures refers to the results obtained with the Na-β″-Al_2O_3 supported catalyst only and has been defined via $U_{WR(Na)} = U_{WR} + 0.65\ V$, in order for the location of the two r_{CH_4} maxima, and thus also for the two TOF_{CH_4} maxima, obtained with the Na-β″-Al_2O_3 and K-β″-Al_2O_3 supports to coincide. This correction is reasonable since the value of U_{WR} for the Na^+ and K^+ ion conducting supports depends on the

coverage of these cations on the reference electrode which cannot be controlled a priori, i.e. during catalyst preparation.

The appearance of this volcano type behavior in the case of the Na-β″-Al_2O_3 and K-β″-Al_2O_3 supports is related to the fact that, as shown already in Figures 2 and 3, the rate vs p_{H_2} and p_{CO_2} curves exhibit local maxima, as analyzed in section 3.1.6.

It is interesting to note in Figure 8 that while TOF_{CH_4} near U_{WR}=0 varies relatively little, less than a factor of five, from one support to another, at the same time TOF_{CO} decreases by almost two orders of magnitude upon comparing the BZY and the alkali conductor supports. This may be attributed to the higher mobility of protons vs alkali ions. Protons can thus migrate easily from the BZY support to the catalyst surface even at U_{WR}=0 and thus can promote CO formation, as experimentally observed. One may thus say that the high mobility of protons leads to a more pronounced metal-support interaction (MSI) for CO formation in this system.

This is consistent with the potential dependence of the selectivities, S_{CH_4} and S_{CO}, depicted in Figure 9. As shown in this figure the selectivity to CH_4, S_{CH_4}, is in general significantly higher for the Na^+ and K^+ conducting supports than for the O^{2-} and H^+ conducting supports and this, in view of Figure 8, is primarily due to the much lower TOF of the CO producing RWGS reaction on Ru supported on the Na^+ and K^+ conducting supports.

3.1.6 Quantitative comparison of the data with the promotional rules

The promotional rules already derived in earlier works [36-38] can be summarized by the inequalities

$$\left(\frac{\partial r}{\partial U_{WR}}\right)\left(\frac{\partial r}{\partial p_D}\right) > 0 \quad ; \quad \left(\frac{\partial r}{\partial U_{WR}}\right)\left(\frac{\partial r}{\partial p_A}\right) < 0 \tag{9}$$

where p_D and p_A stand for the electron donor and electron acceptor reactant. The adsorption of an electron donor/acceptor causes a decrease/increase in work function, Φ, and thus, via eq. (7), to the potential U_{WR}. Consequently the electron donor or

electron acceptor nature of a reactant can be easily determined experimentally by noting the sign of ΔU_{WR} upon adsorption of the reactant.

In the present case the inequalities (9) imply

$$\left(\frac{\partial r}{\partial U_{WR}}\right)\left(\frac{\partial r}{\partial p_{H_2}}\right) > 0 \quad ; \quad \left(\frac{\partial r}{\partial U_{WR}}\right)\left(\frac{\partial r}{\partial p_{CO_2}}\right) < 0 \tag{10}$$

These imply that catalytic rate increases with potential, $(\partial r / \partial U_{WR}) > 0$, when it is positive order in the electron donor reactant i.e. H_2, and negative order in the electron acceptor reactant, i.e. p_{CO_2}. This is the case for the methanation reaction (Figures 2 and 3) and indeed the methanation reaction exhibits $(\partial r_{CH_4} / \partial U_{WR}) > 0$, i.e. electrophobic (or equivalently nucleophilic) behaviour.

On the other hand, according to the same rules (eqs. 9 and 10), a catalytic rate decreases with potential $(\partial r / \partial U_{WR}) < 0$ when it is negative order in the electron donor reactant (i.e. H_2) and positive order in the electron acceptor reactant, i.e. CO_2. As already shown in Figure 4 and 5 this is the case for the reverse water-gas shift reaction (RWGS) which indeed exhibits $(\partial r_{CO} / \partial U_{WR}) < 0$, i.e. electrophilic behaviour (Figure 4, 5 and 7).

Consequently all the rate vs p_{H_2}, rate vs p_{CO_2} and rate vs U_{WR} data are consistent with the promotional rules (eqs. 9 and 10), as shown in Figure 10.

In this figure we have used the data of figures 1 to 5 to compute the parameters

$$\Omega_{CH_4,H_2} = \left(\frac{\partial r_{CH_4}}{\partial U_{WR}}\right)_{p_{H_2},p_{CO_2}} \cdot \left(\frac{\partial r_{CH_4}}{\partial p_{H_2}}\right)_{U_{WR},p_{CO_2}} \tag{11}$$

$$\Omega_{CH_4,CO_2} = \left(\frac{\partial r_{CH_4}}{\partial U_{WR}}\right)_{p_{H_2},p_{CO_2}} \cdot \left(\frac{\partial r_{CH_4}}{\partial p_{CO_2}}\right)_{U_{WR},p_{H_2}} \tag{12}$$

$$\Omega_{CO,H_2} = \frac{\partial r_{CO}}{\partial U_{WR}}\Big)_{p_{H_2},p_{CO_2}} \cdot \left(\frac{\partial r_{CO}}{\partial p_{H_2}}\right)_{U_{WR},p_{CO_2}} \tag{13}$$

$$\Omega_{CO,CO_2} = \left(\frac{\partial r_{CO}}{\partial U_{WR}}\right)_{p_{H_2},p_{CO_2}} \cdot \left(\frac{\partial r_{CO}}{\partial p_{CO_2}}\right)_{U_{WR},p_{H_2}} \tag{14}$$

and to examine if their sign conforms to the predictions of the rules. In fact one observes that for practically all the data it is

$$\Omega_{CH_4,H_2} > 0 \qquad \Omega_{CO,H_2} > 0 \tag{15}$$

$$\Omega_{CH_4,CO_2} < 0 \qquad \Omega_{CO,CO_2} < 0 \tag{16}$$

in very good agreement with equations (9) and (10). Some small deviations occur at small p_{H2} and p_{CO2} values where the rate inevitably becomes first order in H_2 and CO_2 even when negative order dependence is predicted and in fact obtained for higher p_{H2} and p_{CO2} values.

These rules of equations (9) and (10) [36] also predict the observed selectivity dependence on catalyst potential (Fig. 6). Since

$$S_{CH_4} = r_{CH_4} / (r_{CH_4} + r_{CO}) \tag{17}$$

$$S_{CO} = r_{CO} / (r_{CH_4} + r_{CO}) \tag{18}$$

and also

$$(\partial r_{CH_4} / \partial U_{WR}) > 0 \quad , \quad (\partial r_{CO} / \partial U_{WR}) < 0 \tag{19}$$

it follows

$$\partial S_{CH_4} / \partial U_{WR} > 0 \tag{20}$$

$$\partial S_{CO} / \partial U_{WR} < 0 \tag{21}$$

as experimentally observed (Figure 9).

3.2. Catalytic studies of supported catalysts (powders)

Firstly, the monometallic catalysts were tested separately (at atmospheric pressure) (Fig. 11, Fig. 12).

As it is shown in Figures 11 and 12, Co leads to a greater number of hydrocarbon products than Ru, but without achieving the higher methane production rates of the latter. In the following figure (Fig. 13) the results of the bimetallic Ru 5% / Co 15 % w/w / TiO_2 are presented. In Fig. 13 it is demonstrated that the bimetallic catalyst leads to a higher number of hydrocarbons than Co catalyst, preserving the high methane production rates of the Ru catalyst. The effect of this synergy could be clearly observed for every product in Figure 14.

As it is observed in Fig. 15, a pressure raise enhances the production of hydrocarbons, while it undermines the production of CO. Subsequently, the results of the bimetallic catalyst were analysed according to the Schulds - Flory (S-F) polymer chain distribution model. The S-F polymerisation describes a non-selective polymerisation of surface species, through the addition of carbon units, one at a time, at the end of a growing chain. One polymer molecule is produced from each chain, via the addition of a terminating carbon unit. According to this model, every surface species had the same probability of reacting at every stage of the polymerisation, regardless the chain length.The distribution is described by the equation:

$$\log\frac{W_n}{n} = n\log P + \log\frac{(1-P)^2}{P} \qquad (22)$$

Where:

$$P = \frac{DP-1}{DP} \qquad (23)$$

Where Wn is the ratio of the mass of the n-carbon chains to the total mass of the produced hydrocarbons, P chain growth probability and DP the degree of polymerisation.

From the equations it is obtained that log(Wn/n) is a linear function of n and has only one parameter (P, expressed through DP). By plotting our data on a log(Wn/n) VS n chart and by trying several values of DP, the S-F line that describes better the experimental data could be obtained. This analysis is presented in Figure 16.

From Fig. 16, it is observed that the S-F model could not describe well the experimental data. By observing that this anomaly is caused by the deviation of methane, it was assumed that the first step of the polymerisation (C1 → C2) is more difficult than the following ones, so the S-F assumption does not apply for this step. In order to confirm this assumption, the S-F- analysis was repeated, but ignoring the methane this time (assuming ethane as the polymerisation starting point). This analysis is presented in Figure 17.

Where Wn' is the ratio of the mass of the n-carbon chains to the total mass of the produced hydrocarbons excluding methane. From the good agreement of S-F for DP = 1.3 according to the analysis above, we could conclude that the production of n

$\geq$ 2 hydrocarbons could be modeled as a non-selective polymerisation of surface species with the addition of one carbon unit at a time.

4. CONCLUSIONS

The comparative study of the electrochemical promotion of the hydrogenation of CO_2 to CH_4 and CO on Ru catalyst-electrodes deposited or O^{2-}, H^+, Na^+ and K^+ conducting ceramic supports, shows strong similarities and smaller differences between these four catalyst systems. In the case of YSZ and BZY, positive potential application, which corresponds to O^{2-} supply to, or H^+ removal from the catalyst, leads to enhanced rate of methanation and suppressed rate of CO production.

The same suppression of CO production with increasing potential is observed with the Na^+ and K^+ conducting supports. In this case, however, the rate of methanation passes through a maximum with increasing potential, i.e. volcano-type behavior is observed. In all cases the observed promotion behavior is in excellent agreement with the promotional rules of equations (10) and, more generally, equations (9), which can be rationalized both via "through the vacuum" interactions by considering the attractive or repulsive dipole-dipole interactions in the effective double layer present at the metal-gas interface [18, 26, 30, 38], or also via "through the metal" interactions by considering the electron donation and backdonation [30, 38] between the metal and the adsorbed species.

As far as the supported catalysts go, it has been observed that the bimetallic catalyst leads to a large number of hydrocarbon products, preserving the a methane production at the same time. Increasing total pressure enhances the production of hydrocarbons, while it diminishes the production of CO. And finally, the production of $n \geq 2$ hydrocarbons could be modeled as a non-selective polymerisation of surface species according to the Schultz - Flory distribution model.

REFERENCES

[1] W. Wang, S. Wang, X. Ma, J. Gong, Chemical Society Reviews, 40 (2011) 3703-3727.
[2] J. Ma, N. Sun, X. Zhang, N. Zhao, F. Xiao, W. Wei, Y. Sun, Catalysis Today, 148 (2009) 221-231.
[3] U. Rodemerck, M. Holeňa, E. Wagner, Q. Smejkal, A. Barkschat, M. Baerns, ChemCatChem, 5 (2013) 1948-1955.
[4] S. Saeidi, N.A.S. Amin, M.R. Rahimpour, Journal of CO2 Utilization, 5 (2014) 66-81.
[5] M.R. Prairie, A. Renken, J.G. Highfield, K. Ravindranathan Thampi, M. Grätzel, Journal of Catalysis, 129 (1991) 130-144.
[6] S. Sharma, Z. Hu, P. Zhang, E.W. McFarland, H. Metiu, Journal of Catalysis, 278 (2011) 297-309.
[7] S. Tada, O.J. Ochieng, R. Kikuchi, T. Haneda, H. Kameyama, International Journal of Hydrogen Energy, 39 (2014) 10090-10100.
[8] C. Janke, M.S. Duyar, M. Hoskins, R. Farrauto, Applied Catalysis B: Environmental, 152-153 (2014) 184-191.
[9] K. Müller, M. Städter, F. Rachow, D. Hoffmannbeck, D. Schmeißer, Environmental Earth Sciences, 70 (2013) 3771-3778.
[10] G.D. Weatherbee, C.H. Bartholomew, Journal of Catalysis, 87 (1984) 352-362.
[11] Z. Kowalczyk, K. Stołecki, W. Raróg-Pilecka, E. Miśkiewicz, E. Wilczkowska, Z. Karpiński, Applied Catalysis A: General, 342 (2008) 35-39.
[12] M. Marwood, R. Doepper, A. Renken, Applied Catalysis A: General, 151 (1997) 223-246.
[13] P. Panagiotopoulou, D.I. Kondarides, X.E. Verykios, Journal of Physical Chemistry C, 115 (2011) 1220-1230.
[14] P. Panagiotopoulou, D.I. Kondarides, X.E. Verykios, Catalysis Today, 181 (2012) 138-147.
[15] M. Stoukides, C.G. Vayenas, Journal of Catalysis, 70 (1981) 137-146.
[16] C.G. Vayenas, S. Bebelis, S. Ladas, Nature, 343 (1990) 625-627.
[17] J. Pritchard, Nature, 343 (1990) 592-593.
[18] C.G. Vayenas, S. Bebelis, C. Pliangos, S. Brosda, D. Tsiplakides, Electrochemical Activation of Catalysis: Promotion, Electrochemical Promotion and Metal-Support Interactions, Kluwer Academic/Plenum Publishers, New York, 2001.
[19] R.M. Lambert, Electrochemical and Chemical Promotion by Alkalis with Metal Films and Nanoparticles, in: A. Wieckowski, E.R. Savinova, C.G. Vayenas (Eds.) Catalysis and Electrocatalysis at Nanoparticle Surfaces, CRC Press, 2003.
[20] N.A. Anastasijevic, H. Baltruschat, J. Heitbaum, Electrochimica Acta, 38 (1993) 1067-1072.
[21] M.I. Rojas, M.M. Mariscal, E.P.M. Leiva, Electrochimica Acta, 55 (2010) 8673-8679.
[22] C.G. Vayenas, C.G. Koutsodontis, Journal of Chemical Physics, 128 (2008) 182506.
[23] A. Katsaounis, Journal of Applied Electrochemistry, 40 (2010) 885-902.
[24] C.G. Vayenas, Journal of Solid State Electrochemistry, 15 (2011) 1425-1435.
[25] D. Tsiplakides, S. Balomenou, Catalysis Today, 146 (2009) 312-318.
[26] P. Vernoux, L. Lizarraga, M.N. Tsampas, F.M. Sapountzi, A. De Lucas-Consuegra, J.-L. Valverde, S. Souentie, C.G. Vayenas, D. Tsiplakides, S. Balomenou, E.A. Baranova, Chemical Reviews, 113 (2013) 8192-8260.
[27] B.C. Jiménez, d.L.C. Antonio, V.J. Luis, D. Fernando, Caravaca Ángel , C.J. González, One of the Recent Discoveries in Catalysis: The Phenomenon of Electrochemical Promotion in: T.J. C. (Ed.) Advances in Chemistry Research, Nova Science Publishers, 2012.
[28] O.A. Marina, I.V. Yentekakis, C.G. Vayenas, A. Palermo, R.M. Lambert, Journal of Catalysis, 166 (1997) 218-228.
[29] I.V. Yentekakis, G. Moggridge, C.G. Vayenas, R.M. Lambert, Journal of Catalysis, 146 (1994) 292-305.

[30] G. Pacchioni, F. Illas, S.G. Neophytides, C.G. Vayenas, J. Phys. Chem. , 100 (1996) 16653-16661.
[31] C.A. Cavalca, G. Larsen, C.G. Vayenas, G.L. Haller, Journal of Physical Chemistry, 97 (1993) 6115-6119.
[32] A. de Lucas-Consuegra, J. González-Cobos, V. Carcelén, C. Magén, J.L. Endrino, J.L. Valverde, Journal of Catalysis, 307 (2013) 18-26.
[33] M.A. Fortunato, A. Princivalle, C. Capdeillayre, N. Petigny, C. Tardivat, C. Guizard, M.N. Tsampas, F.M. Sapountzi, P. Vernoux, Topics in Catalysis, 57 (2014) 1277-1286.
[34] C.G. Vayenas, R.M. Lambert, S. Ladas, S. Bebelis, S. Neophytides, M.S. Tikhov, N.C. Filkin, M. Makri, D. Tsiplakides, C. Cavalca, K. Besocke, Direct STM, XPS and TPD observation of spillover phenomena over mm distances on metal catalyst films interfaced with solid electrolytes, in: Studies in Surface Science and Catalysis, 1997, pp. 39-47.
[35] X. Li, F. Gaillard, P. Vernoux, Topics in Catalysis, 44 (2007) 391-398.
[36] S. Brosda, C.G. Vayenas, J. Wei, Applied Catalysis B: Environmental, 68 (2006) 109-124.
[37] C.G. Vayenas, S. Brosda, C. Pliangos, Journal of Catalysis, 203 (2001) 329-350.
[38] C. Vayenas, S. Brosda, Top Catal, 57 (2014) 1287-1301.
[39] D. Theleritis, S. Souentie, A. Siokou, A. Katsaounis, C.G. Vayenas, ACS Catalysis, 2 (2012) 770-780.
[40] D. Theleritis, M. Makri, S. Souentie, A. Caravaca, A. Katsaounis, C.G. Vayenas, ChemElectroChem, 1 (2014) 254-262.
[41] M. Makri, A. Katsaounis, C. Vayenas, Electrochimica Acta, (2015) DOI: 10.1016/j.electacta.2015.1003.1144.
[42] I. Kalaitzidou, A. Katsaounis, T. Norby, C.G. Vayenas, Journal of Catalysis, (2015) DOI: 10.1016/j.cat.2015.1008.1023.
[43] C. Benndorf, T.E. Madey, Chemical Physics Letters, 101 (1983) 59-64.
[44] T. Hertel, H. Over, H. Bludau, M. Gierer, G. Ertl, Surface Science, 301 (1994) 1-10.
[45] M. Gierer, H. Bludau, T. Hertel, H. Over, W. Moritz, G. Ertl, Surface Science, 279 (1992) L170-L174.
[46] R.A. DePaola, J. Hrbek, F.M. Hoffmann, The Journal of Chemical Physics, 82 (1985) 2484-2498.
[47] G. Pirug, C. Ritke, H.P. Bonzel, Surface Science, 257 (1991) 50-62.
[48] C.G. Vayenas, S. Bebelis, M. Despotopoulou, Journal of Catalysis, 128 (1991) 415-435.

FIGURE CAPTIONS

Figure 1: Effect of p_{H_2} (a), p_{CO_2} (b) and catalyst potential (c) on the rates of methanation and reverse-water-gas-shift reaction on a Ru/YSZ catalyst. Note the conformity with the promotional rules, i.e. $(\partial r / \partial U_{WR})(\partial r / \partial p_{H_2}) > 0$ and $(\partial r / \partial U_{WR})(\partial r / \partial p_{CO_2}) < 0$, where $\Delta\Phi = e\Delta U_{WR}$ (eq. (7)) [35]. Reprinted with permission from Springer.

Figure 2: Effect of p_{H_2} and of catalyst potential on the rate of CO_2 methanation on the Ru/YSZ, Ru/BZY, Ru/Na-β″-Al_2O_3 and Ru/K-β″-Al_2O_3 catalysts; p_{CO_2} =1 kPa.

Figure 3: Effect of P_{CO2} and of catalyst potential on the rate of CO_2 methanation on the Ru/YSZ, Ru/BZY, Ru/Na-β″-Al_2O_3 and Ru/K-β″-Al_2O_3 catalysts; p_{H_2} =7 kPa.

Figure 4: Effect of p_{H_2} and of catalyst potential on the rate of the RWGS reaction on the Ru/YSZ, Ru/BZY, Ru/Na-β″-Al_2O_3 and Ru/K-β″-Al_2O_3 catalysts; p_{CO_2} =1 kPa.

Figure 5: Effect of P_{CO2} and of catalyst potential the rate of the RWGS reaction on the Ru/YSZ, Ru/BZY, Ru/Na-β″-Al_2O_3 and Ru/K-β″-Al_2O_3 catalysts; p_{H_2} =7 kPa.

Figure 6: Effect of p_{H_2} and of catalyst potential on the selectivities to CH_4 and to CO on the Ru/YSZ, Ru/BZY, Ru/Na-β″-Al_2O_3 and Ru/K-β″-Al_2O_3 catalysts; p_{CO_2} =1 kPa.

Figure 7: Effect of catalyst potential on the rates of CH_4 and CO formation on the Ru/YSZ, Ru/BZY, Ru/Na-β″-Al_2O_3 and Ru/K-β″-Al_2O_3 catalysts; p_{H_2} =7 kPa, p_{CO_2} =1 kPa.

Figure 8: Effect of catalyst potential on the turnover frequencies (TOFs) of CH_4 and CO formation on the Ru/YSZ, Ru/BZY, Ru/Na-β″-Al_2O_3 and Ru/K-β″-Al_2O_3 catalysts; p_{H_2} =7 kPa, p_{CO_2} =1 kPa.

Figure 9: Effect of catalyst potential on the selectivities to CH_4 and to CO on the Ru/YSZ, Ru/BZY, Ru/Na-β″-Al_2O_3 and Ru/K-β″-Al_2O_3 catalysts; p_{H_2} =7 kPa, p_{CO_2} =1 kPa

Figure 10: (a) Effect of p_{H2} on the sign of the parameter Ω_{CH_4,H_2} defined in equation (11) obtained from the data of Figure 2 for the four different supports. **(b)** Effect of p_{CO_2} on the sign of the parameter Ω_{CH_4,CO_2} defined in equation (12) obtained from the data of Figure 3. **(c)** Effect of p_{H_2} on the sign of the parameter Ω_{CO,H_2} defined in equation (13) obtained from the data of Figure 4. **(d)** Effect of p_{CO_2} on the sign of the parameter Ω_{CO,CO_2} defined in equation (14) obtained from the data of Figure 5.

Figure 11: Effect of temperature on CH_4 and CO production rates, using 200 mg of Ru 5% w/w / TiO_2 catalyst under atmospheric pressure (P = 1bar).

Figure 12: Effect of temperature on hydrocarbons and CO production rates, using 200 mg of Co 15% w/w / TiO_2 catalyst under atmospheric pressure (P = 1bar).

Figure 13: Effect of temperature on ηydrocarbons and CO production rates, using 200 mg of Ru 2% / Co 15% w/w / TiO_2 catalyst under atmospheric pressure (P = 1bar).

Figure 14: Effect of the synergy of the catalysts on the hydrocarbons and CO production rates, using 200 mg of Ru 2% / Co 15% w/w / TiO_2 catalyst under atmospheric pressure (P = 1bar).

Figure 15: Effect of temperature on *hydrocarbons and CO production rates, using 200 mg of Ru 2% / Co 15% w/w / TiO_2 catalyst for several pressure values (in bar).*

Figure 16: Schultz – Flory analysis for the experimental data of the Ru 2% / Co 15% w/w / TiO_2 catalyst, where DP = 1.12 is obtained.

Figure 17: Schultz – Flory analysis for the experimental data of the Ru 2% / Co 15% w/w / TiO_2 catalyst (ignoring the methane), where DP = 1.3 is obtained.

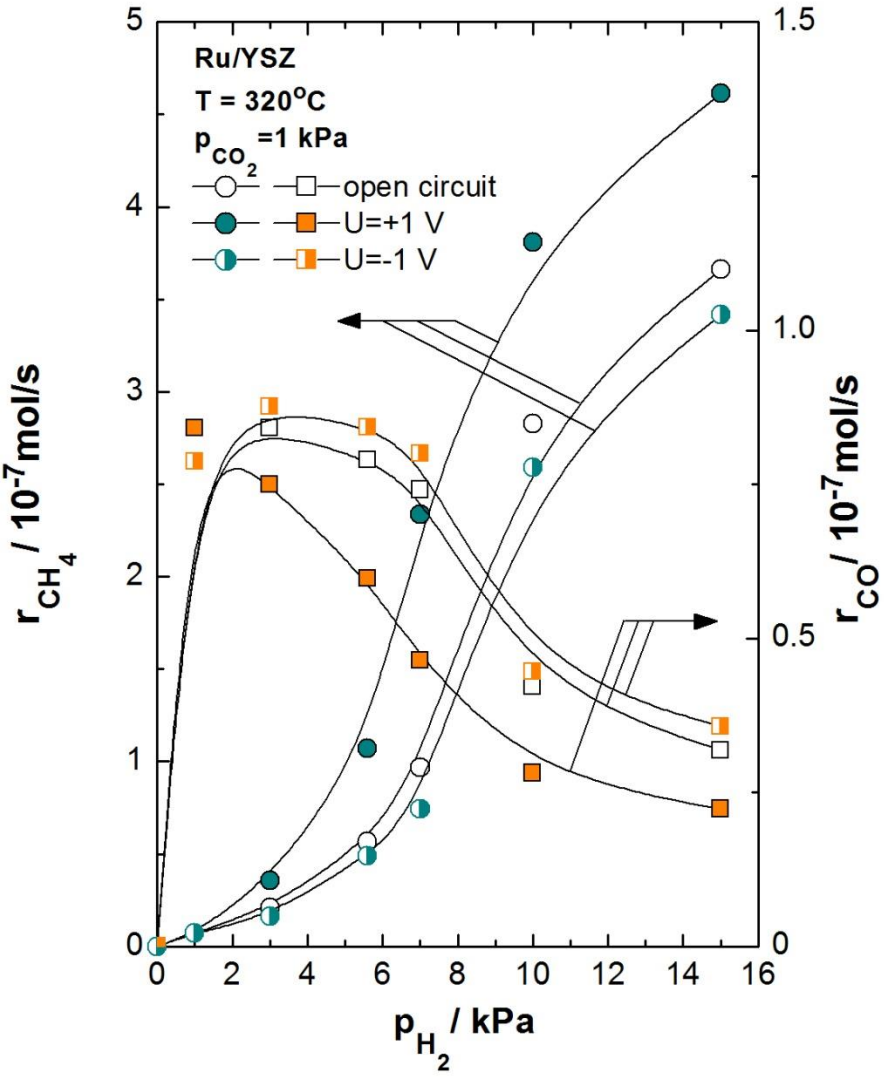
Ru/YSZ
T = 320°C
p_CO2 =1 kPa
open circuit
U=+1 V
U=-1 V
r_CH4 / 10^-7 mol/s
r_CO / 10^-7 mol/s
p_H2 / kPa
0
1
2
3
4
5
0
0.5
1.0
1.5
0
2
4
6
8
10
12
14
16

Figure 1a

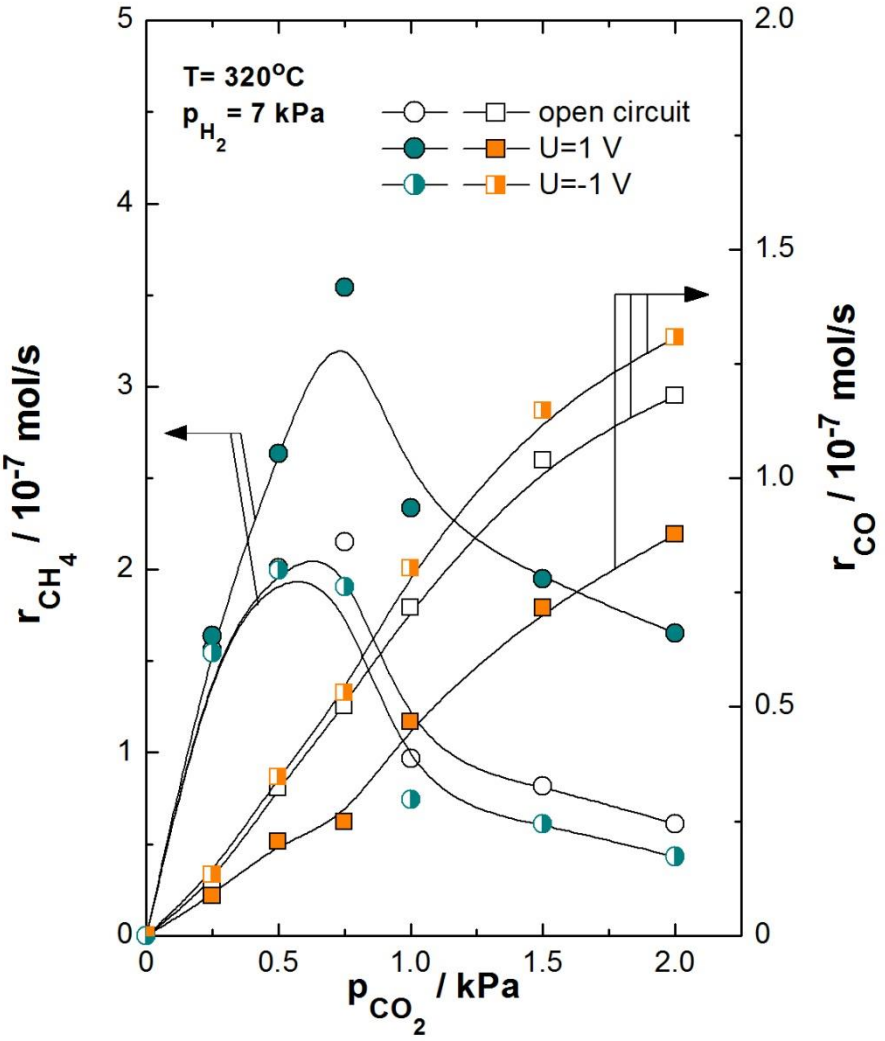
T= 320°C
p_H2 = 7 kPa
open circuit
U=1 V
U=-1 V
r_CH4 / 10^-7 mol/s
r_CO / 10^-7 mol/s
p_CO2 / kPa
0
0.5
1.0
1.5
2.0
1
2
3
4
5

Figure 1b

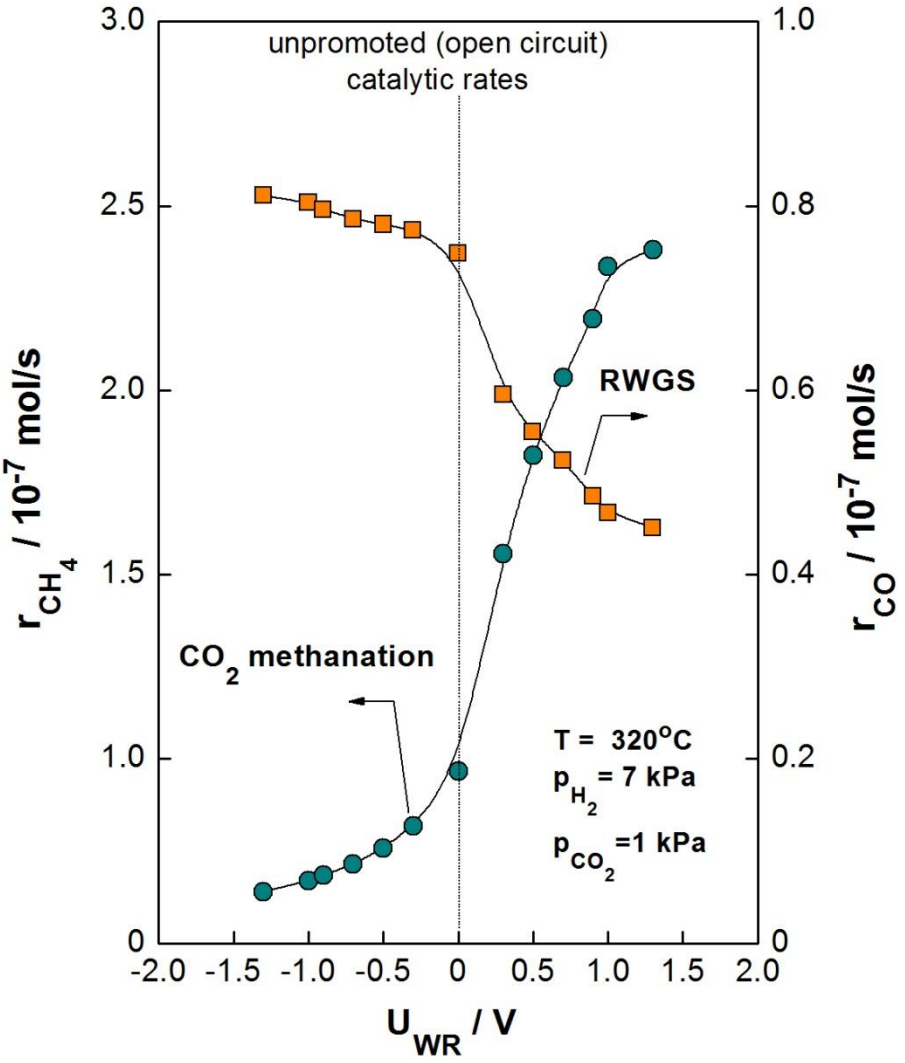
unpromoted (open circuit)
catalytic rates
RWGS
CO2 methanation
T = 320°C
pH2 = 7 kPa
pCO2 =1 kPa
rCH4 / 10-7 mol/s
rCO / 10-7 mol/s
UWR / V
3.0
2.5
2.0
1.5
1.0
0
1.0
0.8
0.6
0.4
0.2
0
-2.0 -1.5 -1.0 -0.5 0 0.5 1.0 1.5 2.0

Figure 1c

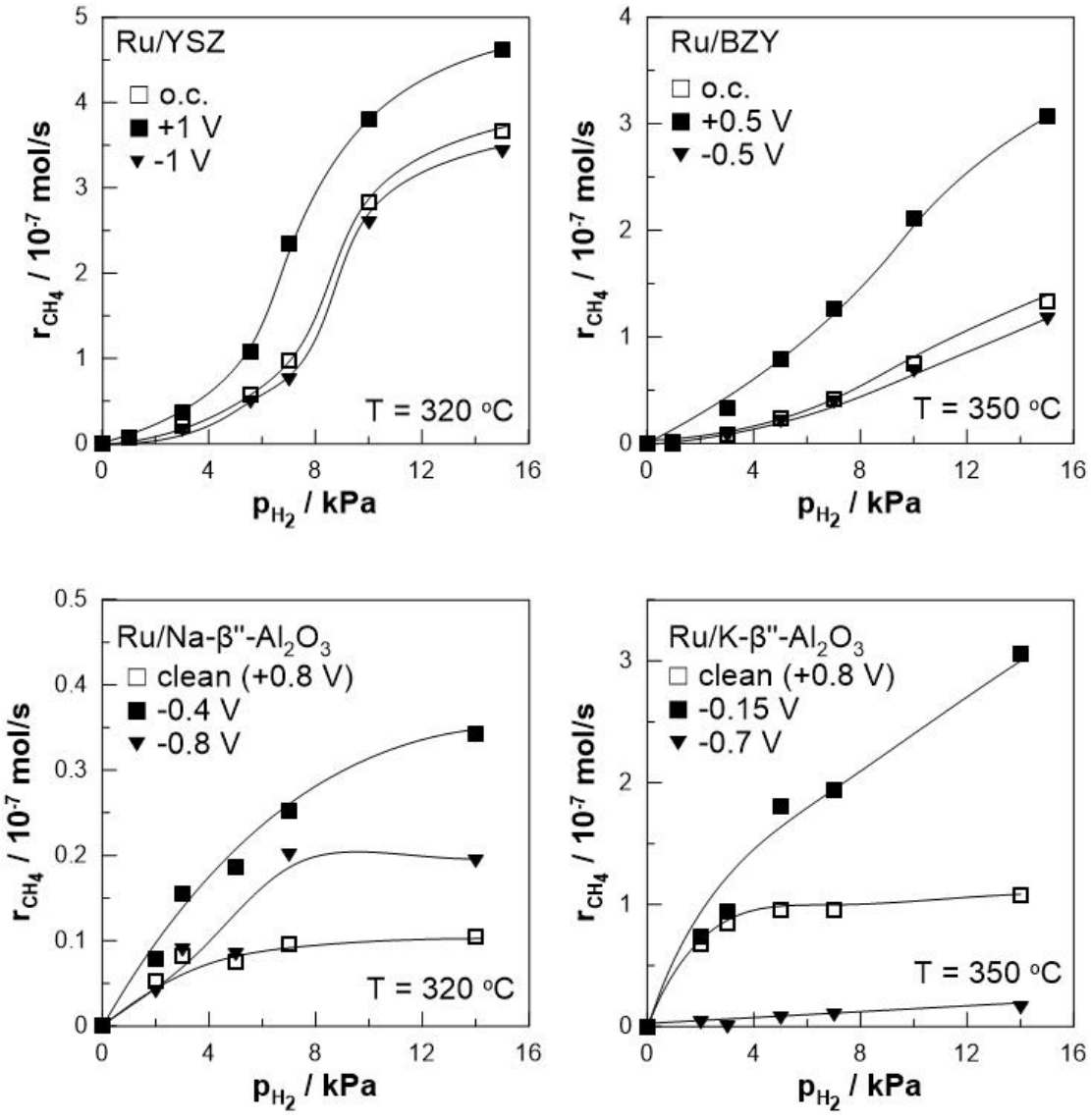
Ru/YSZ
o.c.
+1 V
-1 V
T = 320 °C
r_{CH_4} / 10^{-7} mol/s
p_{H_2} / kPa
Ru/BZY
o.c.
+0.5 V
-0.5 V
T = 350 °C
r_{CH_4} / 10^{-7} mol/s
p_{H_2} / kPa
Ru/Na-β''-Al_2O_3
clean (+0.8 V)
-0.4 V
-0.8 V
T = 320 °C
r_{CH_4} / 10^{-7} mol/s
p_{H_2} / kPa
Ru/K-β''-Al_2O_3
clean (+0.8 V)
-0.15 V
-0.7 V
T = 350 °C
r_{CH_4} / 10^{-7} mol/s
p_{H_2} / kPa

Figure 2

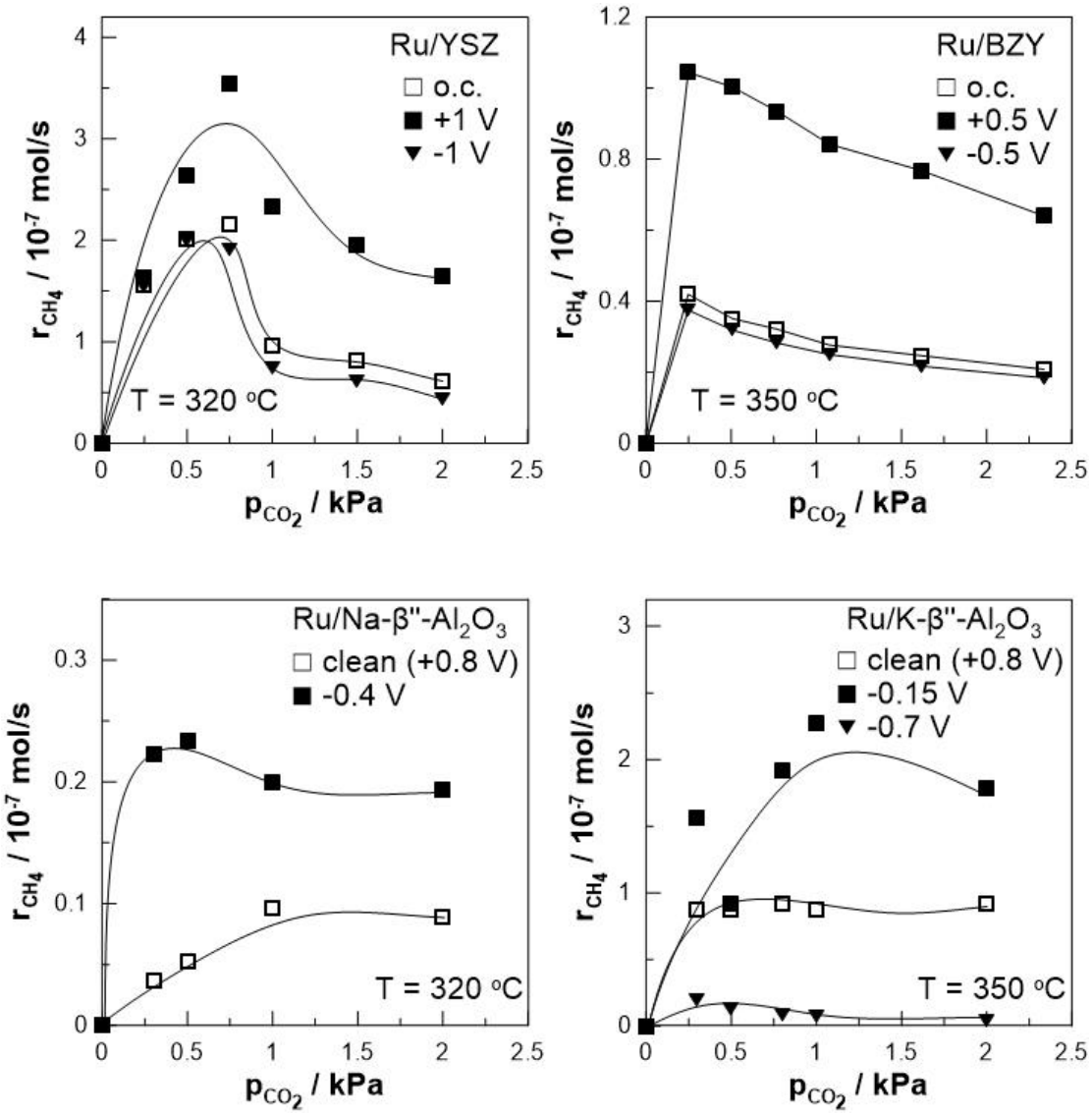
Ru/YSZ
o.c.
+1 V
-1 V
T = 320 °C
r_{CH_4} / 10^{-7} mol/s
p_{CO_2} / kPa
Ru/BZY
o.c.
+0.5 V
-0.5 V
T = 350 °C
r_{CH_4} / 10^{-7} mol/s
p_{CO_2} / kPa
Ru/Na-β''-Al_2O_3
clean (+0.8 V)
-0.4 V
T = 320 °C
r_{CH_4} / 10^{-7} mol/s
p_{CO_2} / kPa
Ru/K-β''-Al_2O_3
clean (+0.8 V)
-0.15 V
-0.7 V
T = 350 °C
r_{CH_4} / 10^{-7} mol/s
p_{CO_2} / kPa

Figure 3

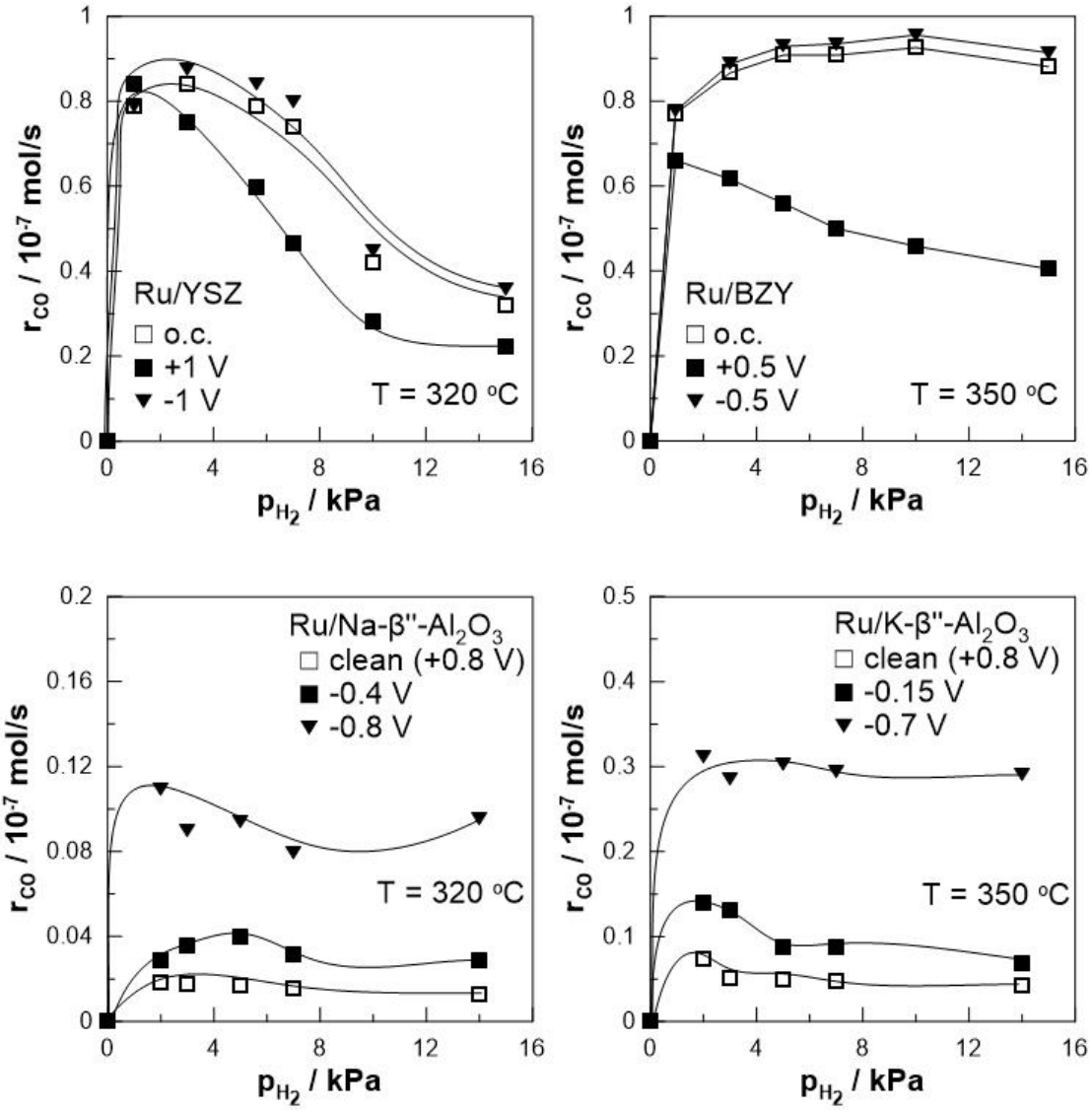
Ru/YSZ
o.c.
+1 V
-1 V
T = 320 °C
Ru/BZY
o.c.
+0.5 V
-0.5 V
T = 350 °C
Ru/Na-β''-Al2O3
clean (+0.8 V)
-0.4 V
-0.8 V
T = 320 °C
Ru/K-β''-Al2O3
clean (+0.8 V)
-0.15 V
-0.7 V
T = 350 °C
rCO / 10-7 mol/s
pH2 / kPa

Figure 4

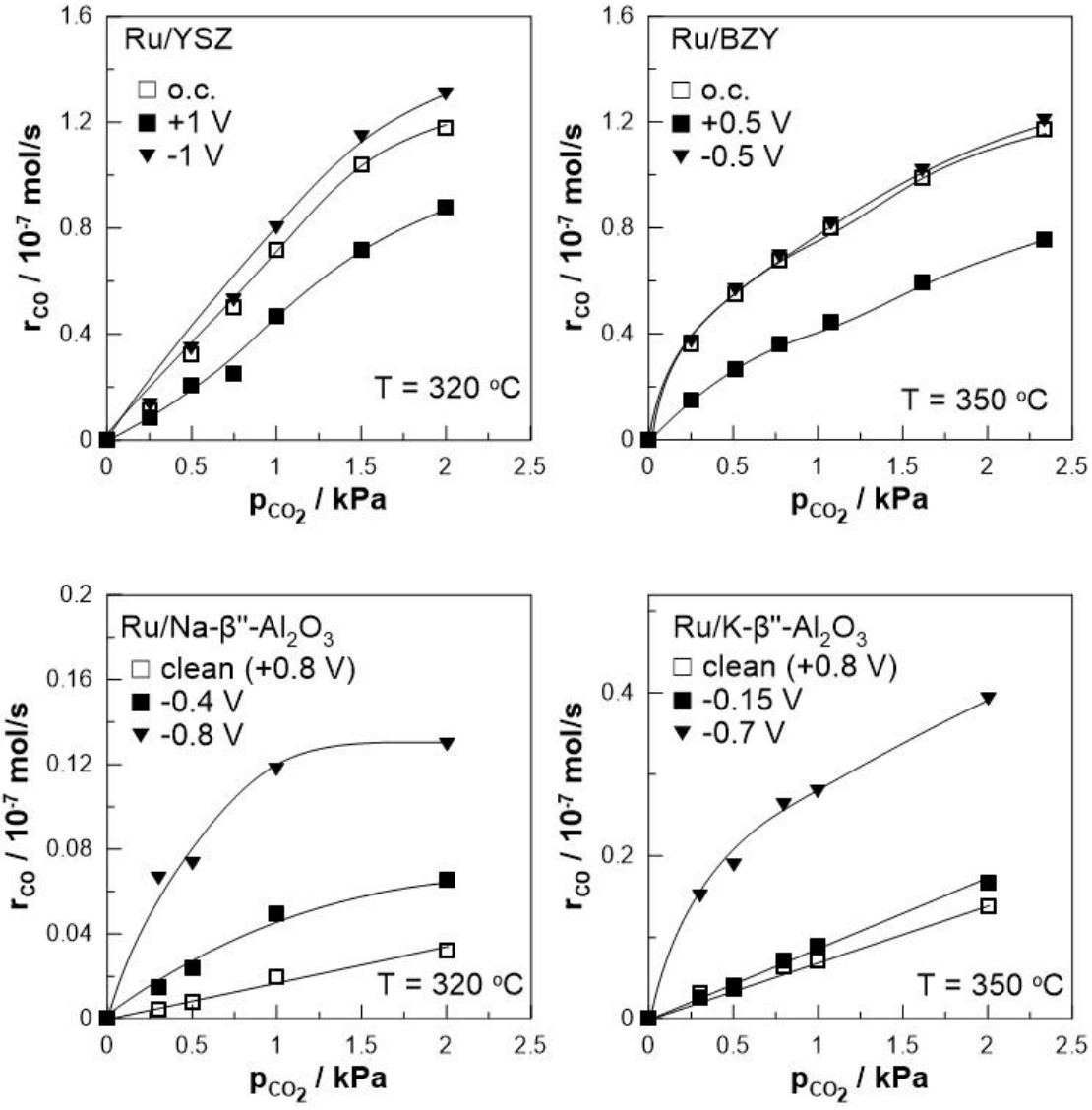
Ru/YSZ
o.c.
+1 V
-1 V
T = 320 °C
Ru/BZY
o.c.
+0.5 V
-0.5 V
T = 350 °C
Ru/Na-β''-Al2O3
clean (+0.8 V)
-0.4 V
-0.8 V
T = 320 °C
Ru/K-β''-Al2O3
clean (+0.8 V)
-0.15 V
-0.7 V
T = 350 °C
r_CO / 10^-7 mol/s
p_CO2 / kPa

Figure 5

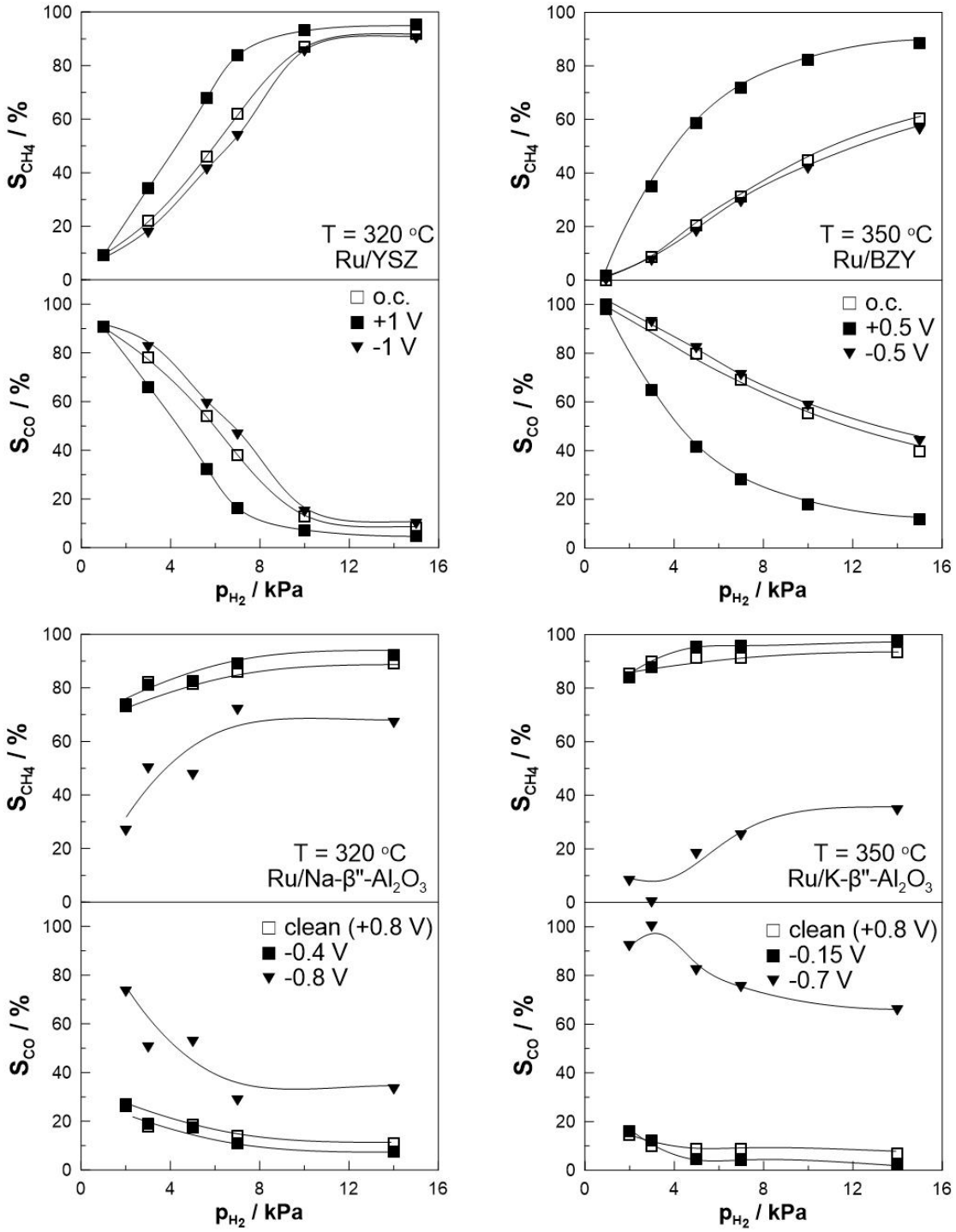
T = 320 °C
Ru/YSZ
□ o.c.
■ +1 V
▼ -1 V
T = 350 °C
Ru/BZY
□ o.c.
■ +0.5 V
▼ -0.5 V
T = 320 °C
Ru/Na-β"-Al2O3
□ clean (+0.8 V)
■ -0.4 V
▼ -0.8 V
T = 350 °C
Ru/K-β"-Al2O3
□ clean (+0.8 V)
■ -0.15 V
▼ -0.7 V
S_CH4 / %
S_CO / %
p_H2 / kPa

Figure 6

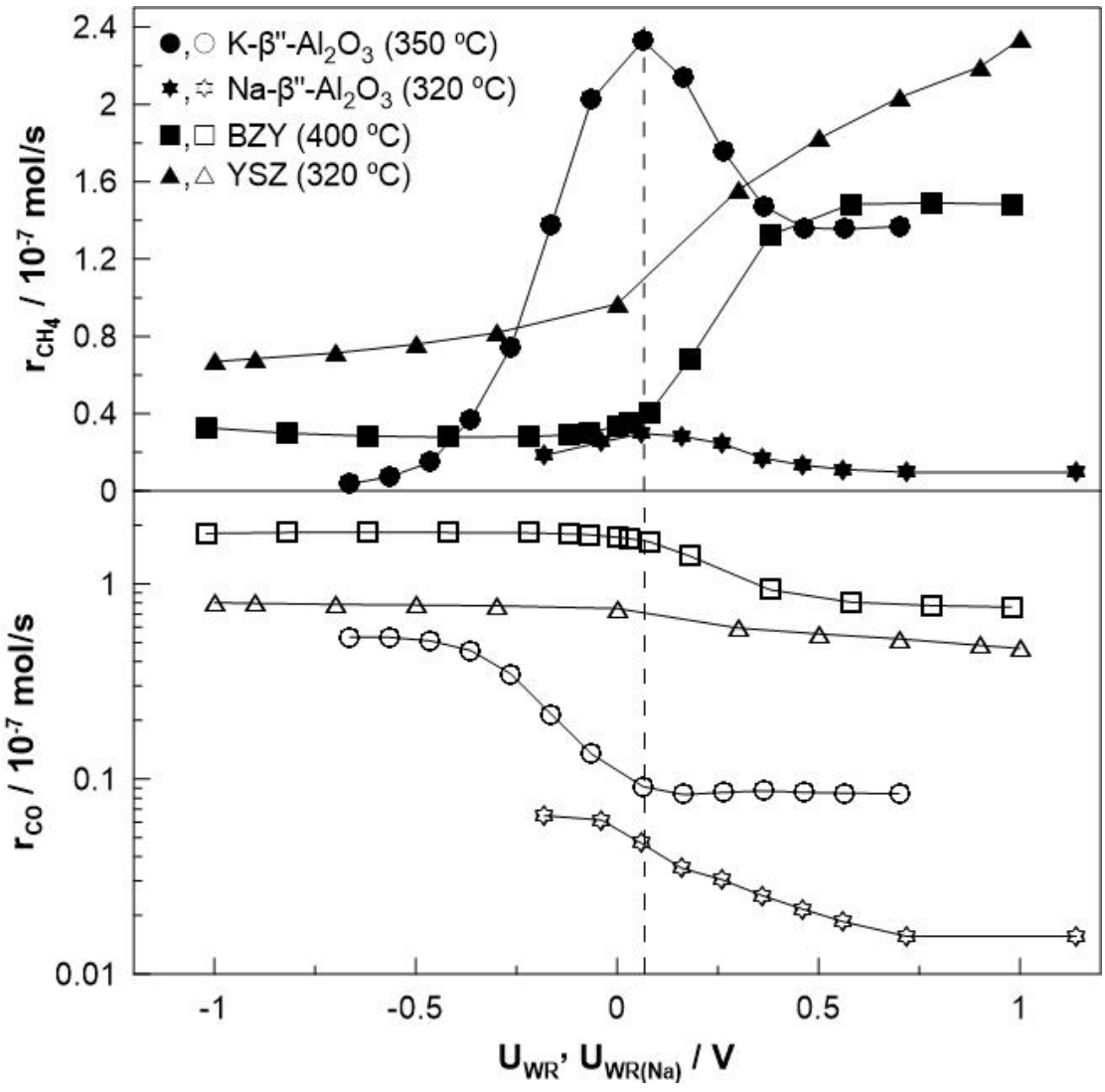
●,○ K-β''-Al2O3 (350 °C)
★,☆ Na-β''-Al2O3 (320 °C)
■,□ BZY (400 °C)
▲,△ YSZ (320 °C)
r_CH4 / 10^-7 mol/s
r_CO / 10^-7 mol/s
U_WR, U_WR(Na) / V

Figure 7

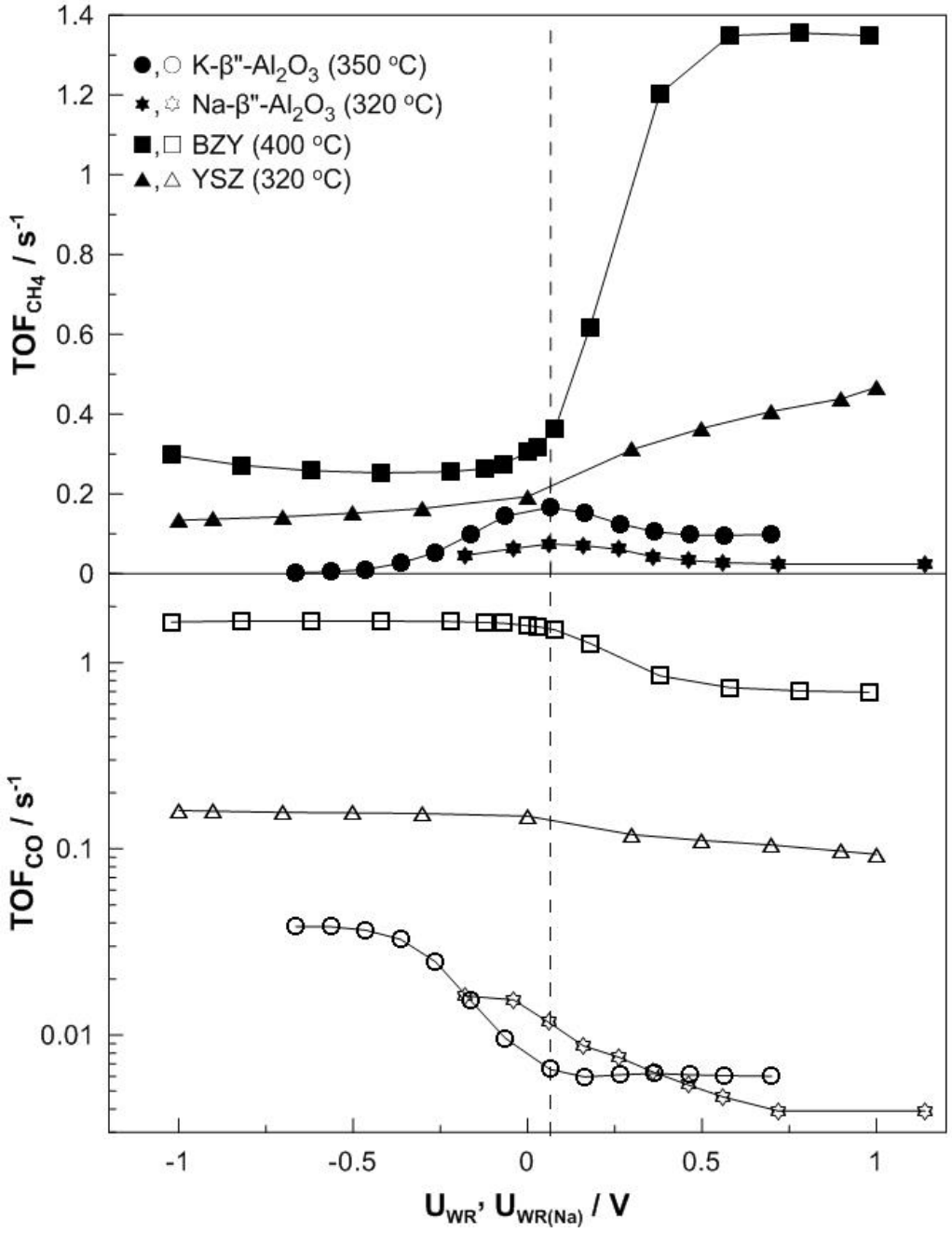
●,○ K-β"-Al2O3 (350 °C)
★,☼ Na-β"-Al2O3 (320 °C)
■,□ BZY (400 °C)
▲,△ YSZ (320 °C)
TOFCH4 / s-1
TOFCO / s-1
UWR, UWR(Na) / V
1.4
1.2
1
0.8
0.6
0.4
0.2
0
0.1
0.01
-1
-0.5
0
0.5
1

Figure 8

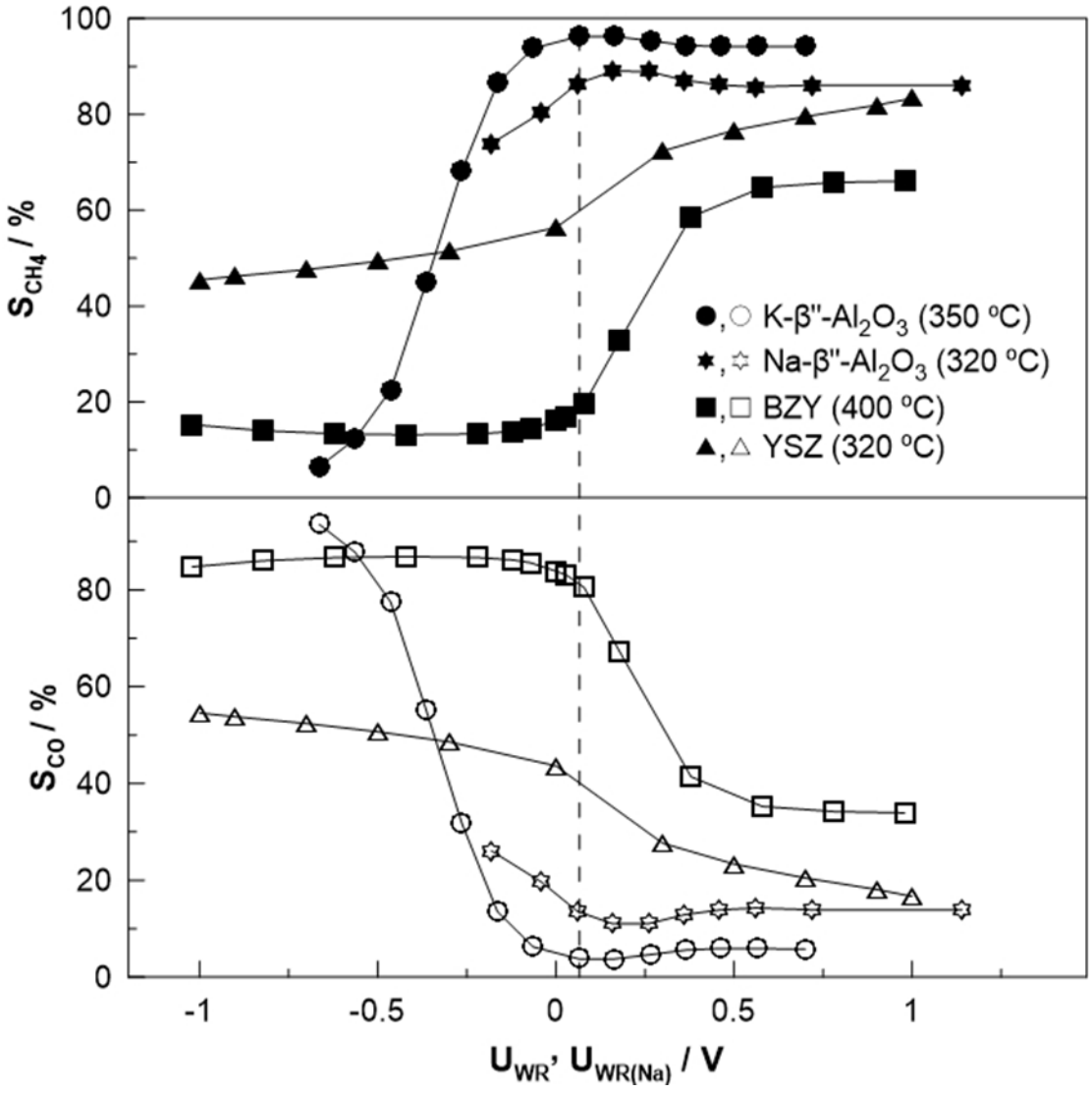
100
80
60
40
20
0
S_{CH_4} / %
●,○ K-β''-Al_2O_3 (350 °C)
★,☆ Na-β''-Al_2O_3 (320 °C)
■,□ BZY (400 °C)
▲,△ YSZ (320 °C)
80
60
40
20
0
S_{CO} / %
-1
-0.5
0
0.5
1
U_{WR}, $U_{WR(Na)}$ / V

Figure 9

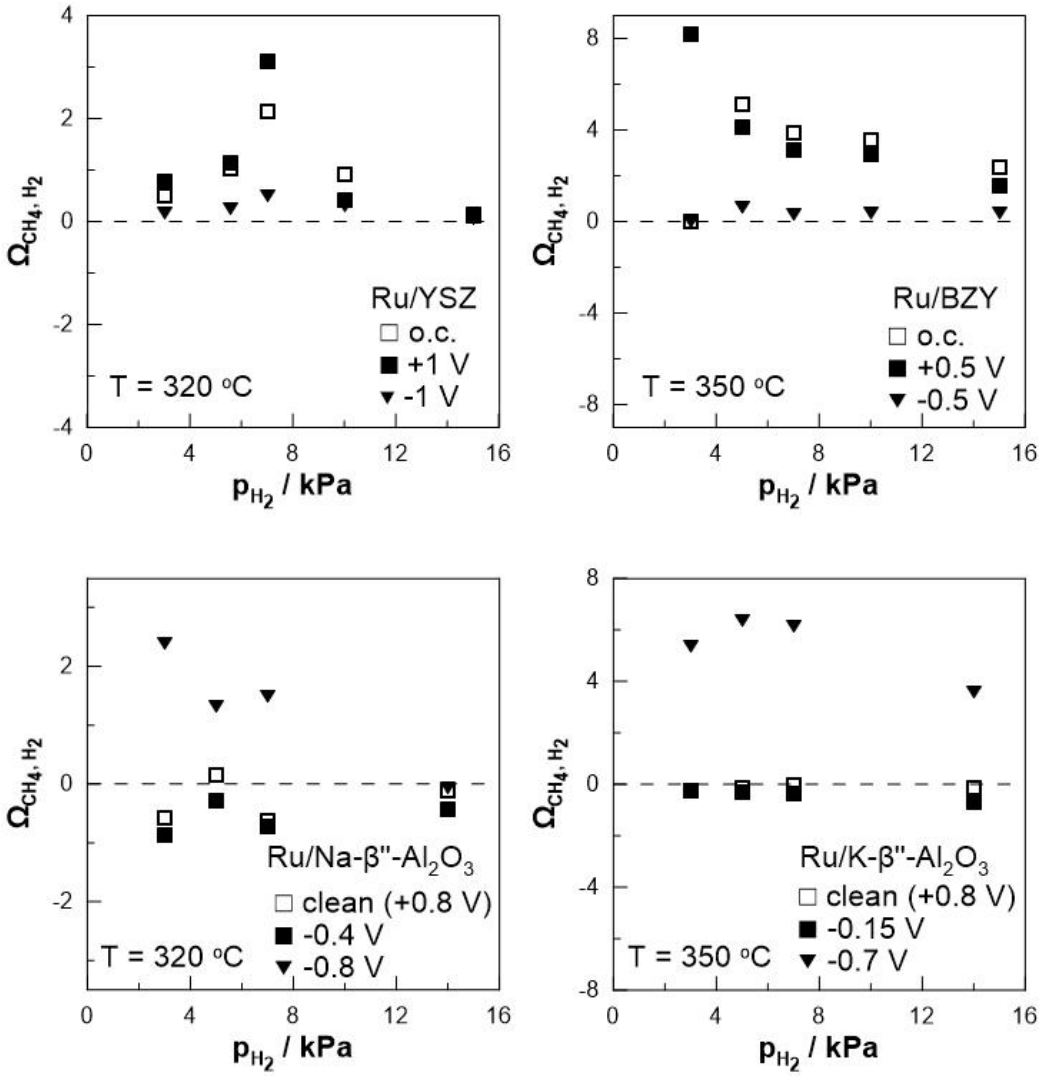
Ru/YSZ
o.c.
+1 V
-1 V
T = 320 °C
Ru/BZY
o.c.
+0.5 V
-0.5 V
T = 350 °C
Ru/Na-β''-Al2O3
clean (+0.8 V)
-0.4 V
-0.8 V
T = 320 °C
Ru/K-β''-Al2O3
clean (+0.8 V)
-0.15 V
-0.7 V
T = 350 °C
ΩCH4, H2
pH2 / kPa

Figure 10a

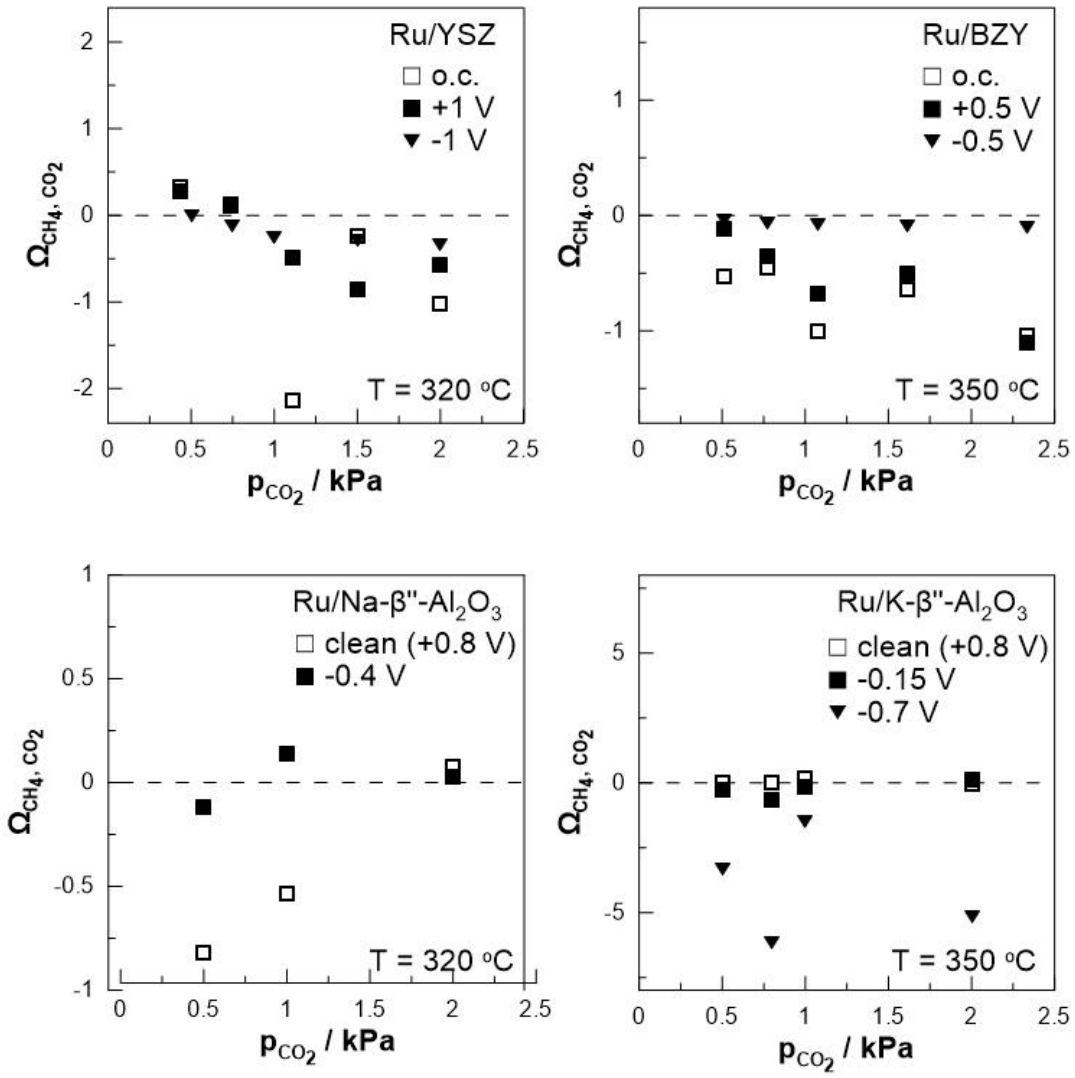
Ru/YSZ
o.c.
+1 V
-1 V
T = 320 °C
Ru/BZY
o.c.
+0.5 V
-0.5 V
T = 350 °C
Ru/Na-β''-Al2O3
clean (+0.8 V)
-0.4 V
T = 320 °C
Ru/K-β''-Al2O3
clean (+0.8 V)
-0.15 V
-0.7 V
T = 350 °C
ΩCH4, CO2
pCO2 / kPa

Figure 10b

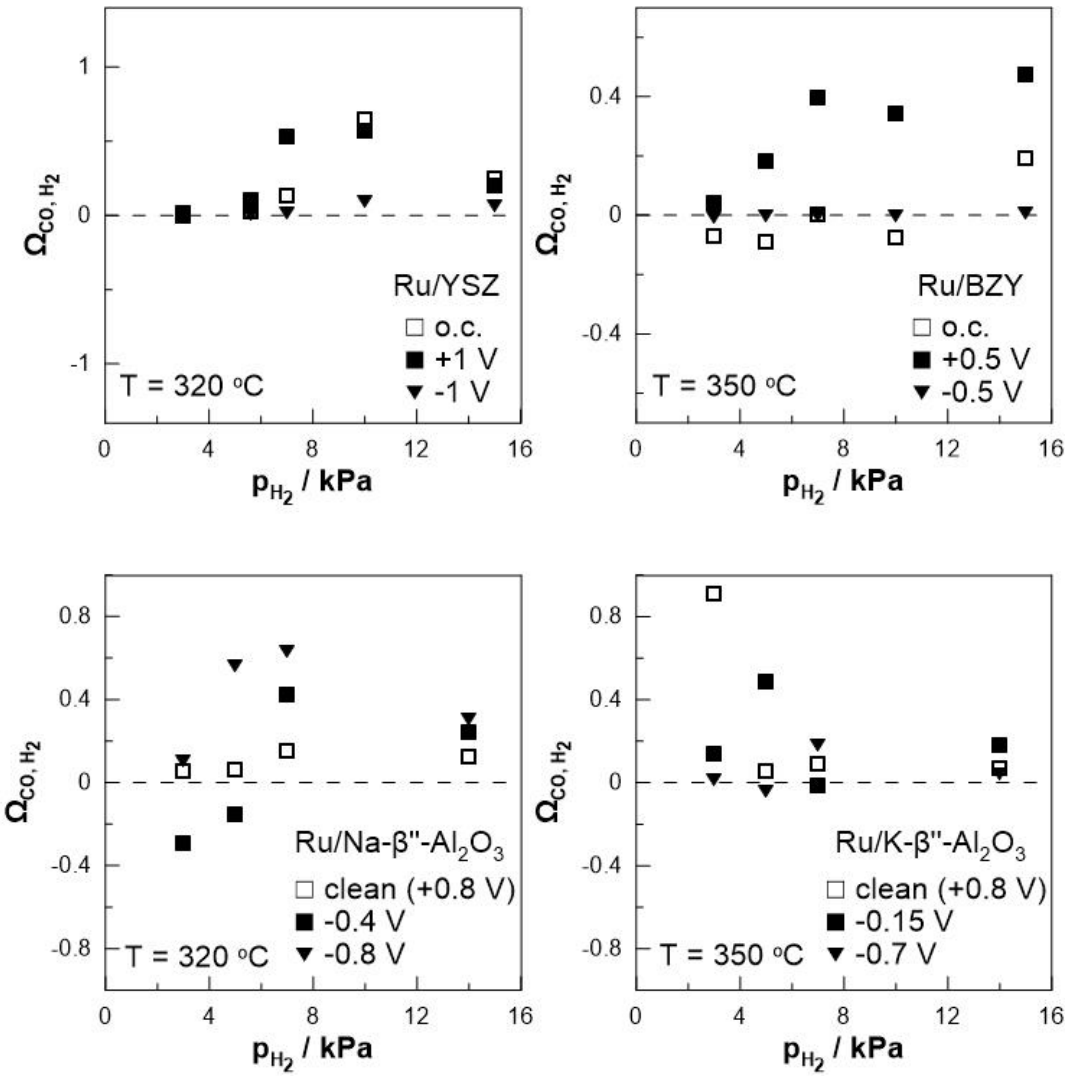
Ru/YSZ
o.c.
+1 V
-1 V
T = 320 °C
Ru/BZY
o.c.
+0.5 V
-0.5 V
T = 350 °C
Ru/Na-β''-Al2O3
clean (+0.8 V)
-0.4 V
-0.8 V
T = 320 °C
Ru/K-β''-Al2O3
clean (+0.8 V)
-0.15 V
-0.7 V
T = 350 °C
ΩCO, H2
pH2 / kPa

Figure 10c

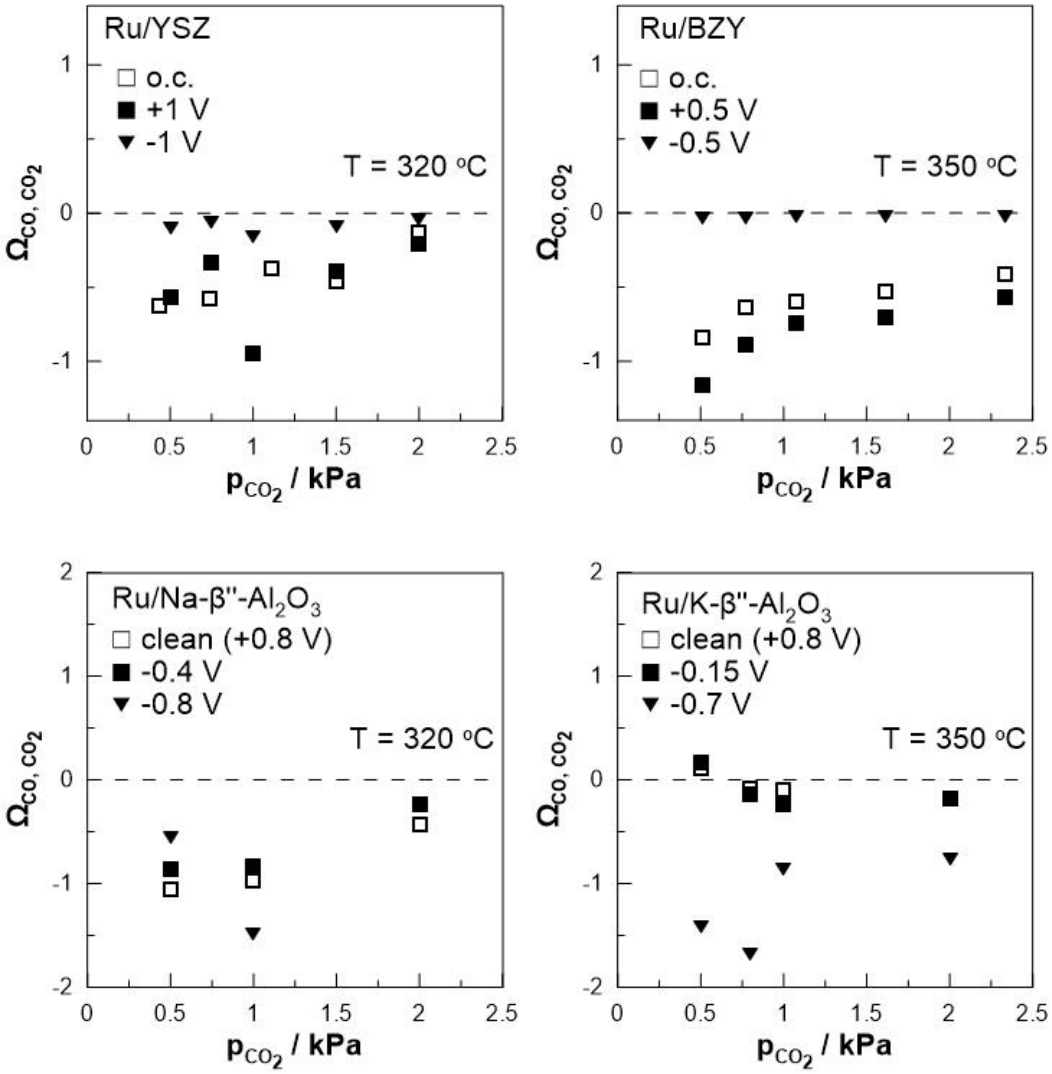
Ru/YSZ
o.c.
+1 V
-1 V
T = 320 °C
Ru/BZY
o.c.
+0.5 V
-0.5 V
T = 350 °C
Ru/Na-β''-Al2O3
clean (+0.8 V)
-0.4 V
-0.8 V
T = 320 °C
Ru/K-β''-Al2O3
clean (+0.8 V)
-0.15 V
-0.7 V
T = 350 °C
Ωco, co2
pco2 / kPa

Figure 10d

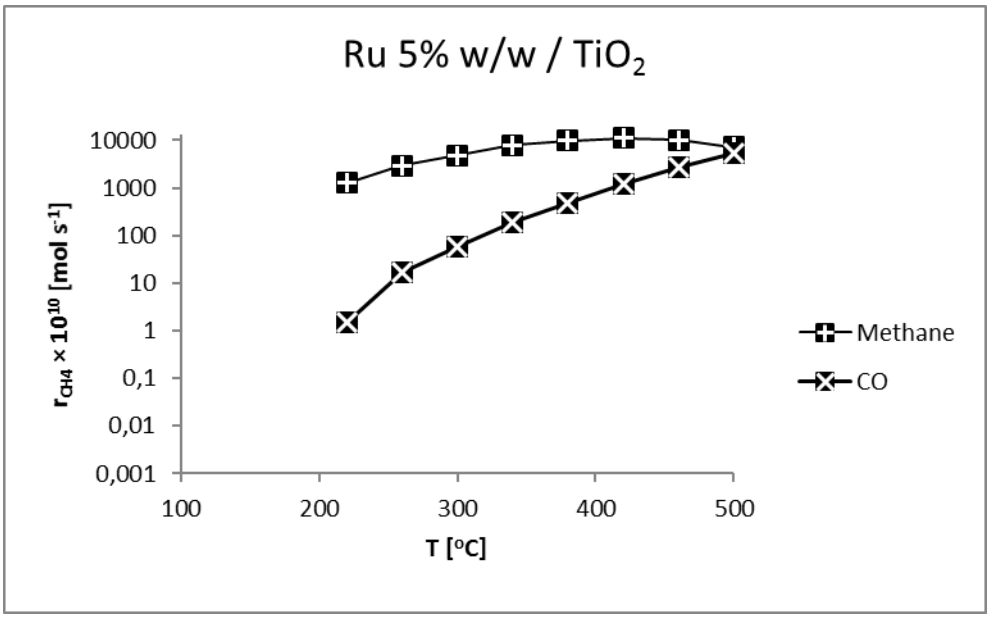
Ru 5% w/w / TiO2
10000
1000
100
10
1
0,1
0,01
0,001
r_CH4 × 10^10 [mol s^-1]
100
200
300
400
500
T [°C]
Methane
CO

Figure 11

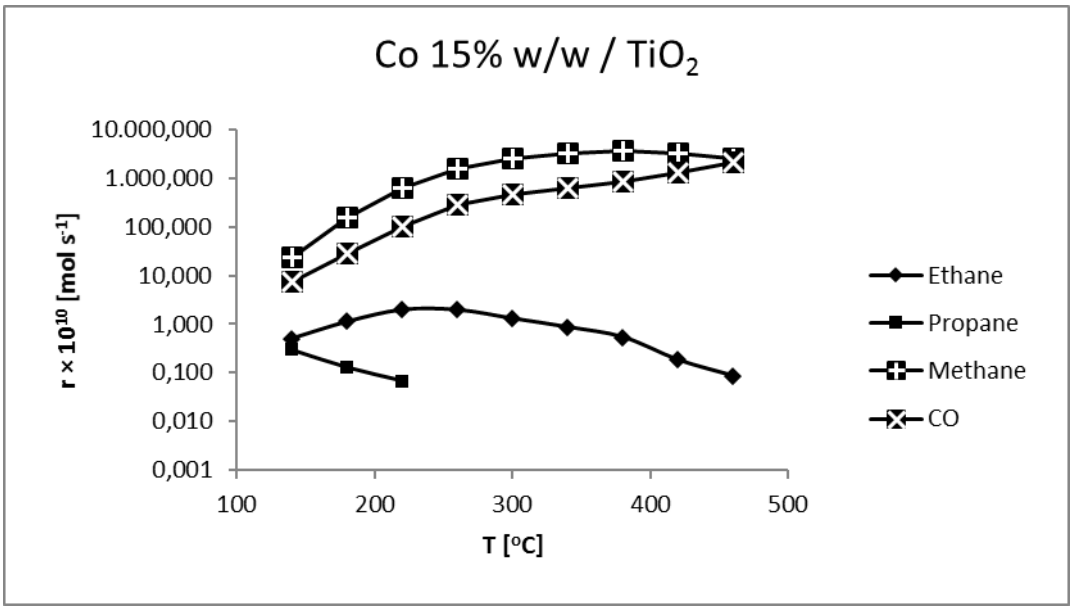
Co 15% w/w / TiO2
10.000,000
1.000,000
100,000
10,000
1,000
0,100
0,010
0,001
r × 10^10 [mol s^-1]
100
200
300
400
500
T [ºC]
Ethane
Propane
Methane
CO

Figure 12

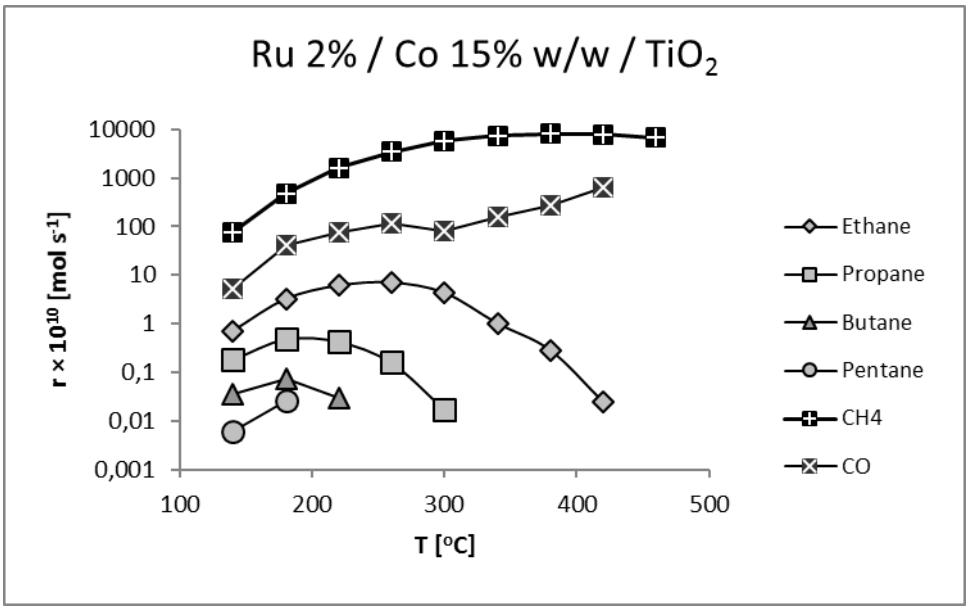
Ru 2% / Co 15% w/w / TiO2
r × 10^10 [mol s^-1]
10000
1000
100
10
1
0,1
0,01
0,001
100
200
300
400
500
T [°C]
Ethane
Propane
Butane
Pentane
CH4
CO

Figure 13

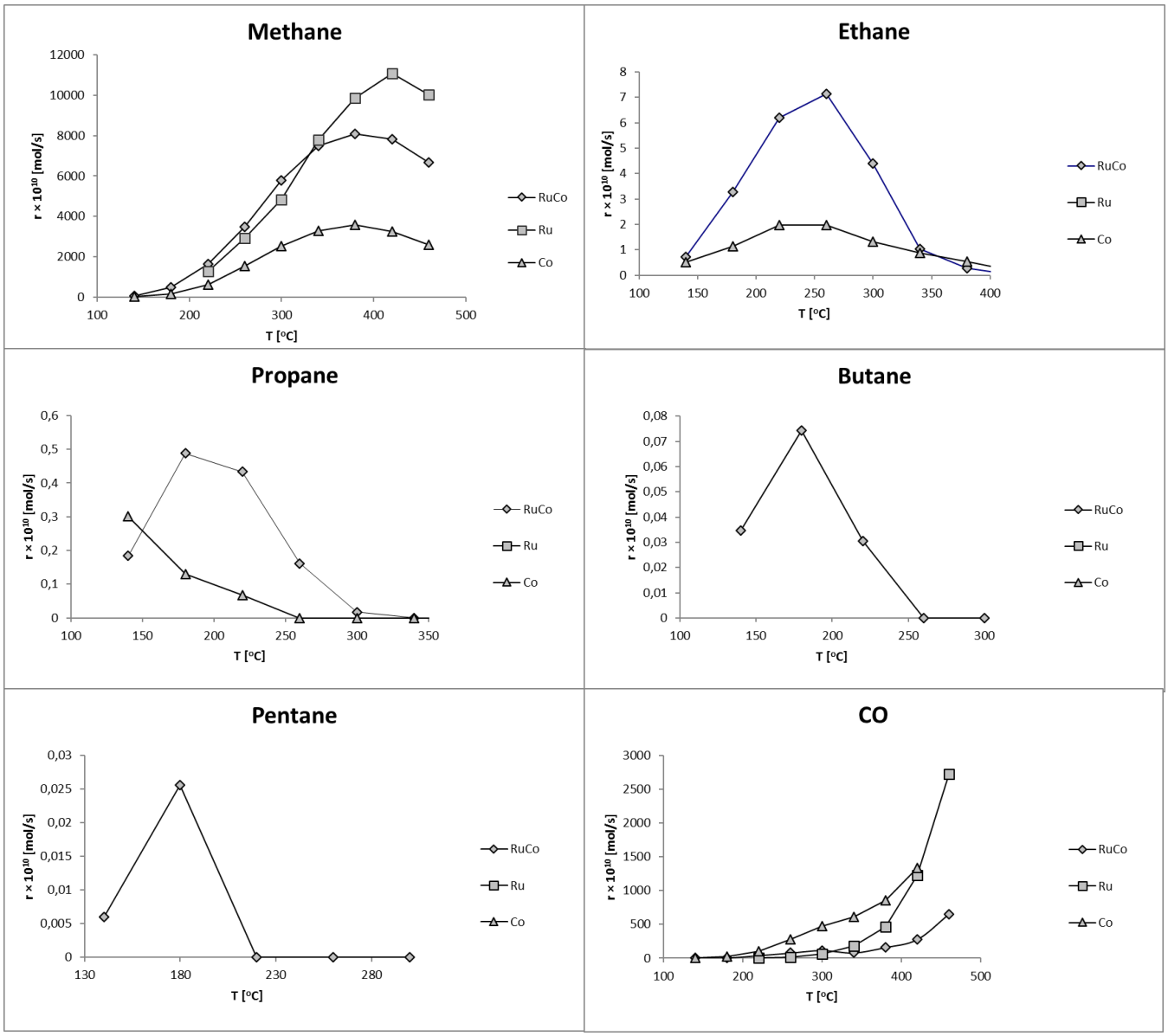
Methane
r × 10¹⁰ [mol/s]
T [°C]
RuCo
Ru
Co
Ethane
r × 10¹⁰ [mol/s]
T [°C]
RuCo
Ru
Co
Propane
r × 10¹⁰ [mol/s]
T [°C]
RuCo
Ru
Co
Butane
r × 10¹⁰ [mol/s]
T [°C]
RuCo
Ru
Co
Pentane
r × 10¹⁰ [mol/s]
T [°C]
RuCo
Ru
Co
CO
r × 10¹⁰ [mol/s]
T [°C]
RuCo
Ru
Co

Figure 14

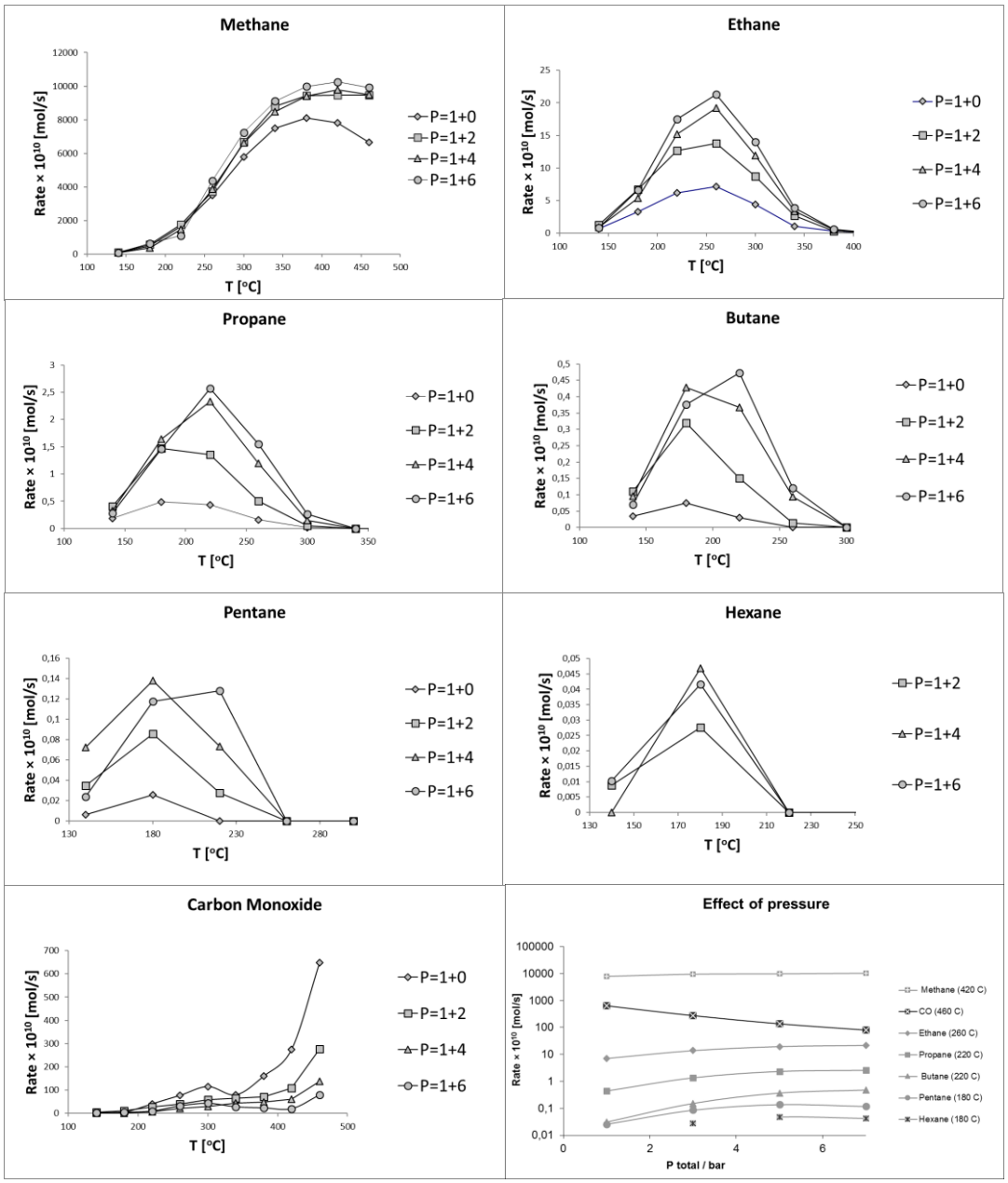
Methane
Rate × 10¹⁰ [mol/s]
T [°C]
P=1+0
P=1+2
P=1+4
P=1+6
Ethane
Rate × 10¹⁰ [mol/s]
T [°C]
P=1+0
P=1+2
P=1+4
P=1+6
Propane
Rate × 10¹⁰ [mol/s]
T [°C]
P=1+0
P=1+2
P=1+4
P=1+6
Butane
Rate × 10¹⁰ [mol/s]
T [°C]
P=1+0
P=1+2
P=1+4
P=1+6
Pentane
Rate × 10¹⁰ [mol/s]
T [°C]
P=1+0
P=1+2
P=1+4
P=1+6
Hexane
Rate × 10¹⁰ [mol/s]
T [°C]
P=1+2
P=1+4
P=1+6
Carbon Monoxide
Rate × 10¹⁰ [mol/s]
T [°C]
P=1+0
P=1+2
P=1+4
P=1+6
Effect of pressure
Rate × 10¹⁰ [mol/s]
P total / bar
Methane (420 C)
CO (460 C)
Ethane (260 C)
Propane (220 C)
Butane (220 C)
Pentane (180 C)
Hexane (180 C)

Figure 15

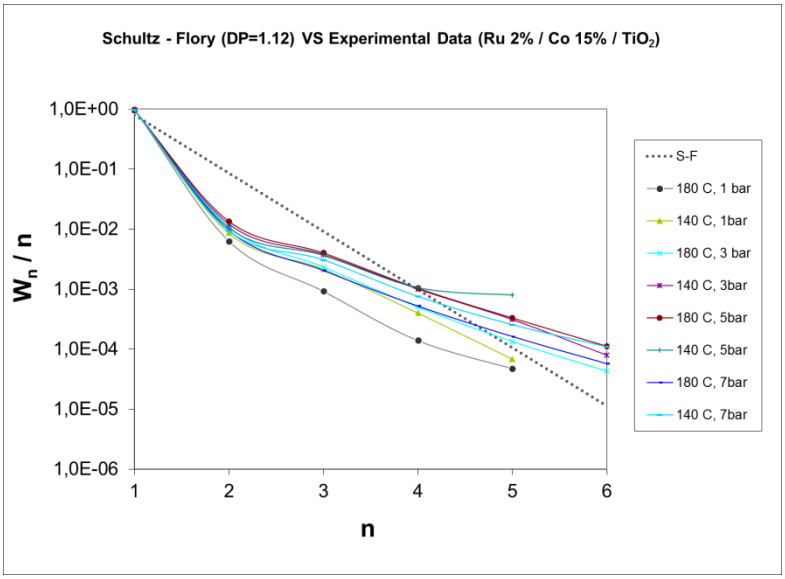
Schultz - Flory (DP=1.12) VS Experimental Data (Ru 2% / Co 15% / TiO2)
1,0E+00
1,0E-01
1,0E-02
1,0E-03
1,0E-04
1,0E-05
1,0E-06
Wn / n
1
2
3
4
5
6
n
S-F
180 C, 1 bar
140 C, 1bar
180 C, 3 bar
140 C, 3bar
180 C, 5bar
140 C, 5bar
180 C, 7bar
140 C, 7bar

Figure 16

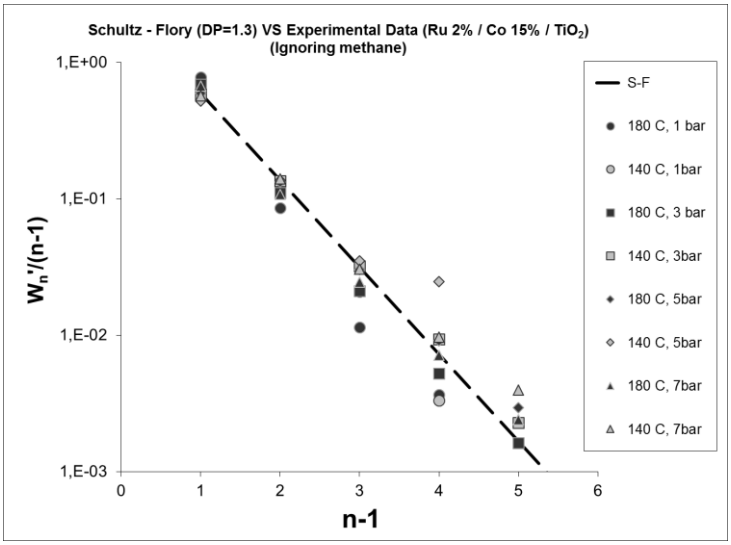

Figure 17

European Union
European Social Fund
OPERATIONAL PROGRAMME
EDUCATION AND LIFELONG LEARNING
investing in knowledge society
MINISTRY OF EDUCATION & RELIGIOUS AFFAIRS
MANAGING AUTHORITY
NSRF 2007-2013
programme for development
EUROPEAN SOCIAL FUND
Co- financed by Greece and the European Union

This project is implemented under the "ARISTEIA I" Action (467) of the "OPERATIONAL PROGRAMME EDUCATION AND LIFELONG LEARNING" and is co-funded by the European Social Fund (ESF) and National Resources.